This is a repository copy of *HpARI protein secreted by a helminth parasite suppresses interleukin-33*.

White Rose Research Online URL for this paper:
https://eprints.whiterose.ac.uk/122893/

Version: Accepted Version

Article:

1 **HpARI protein secreted by a helminth parasite suppresses interleukin-33**

2

3 Megan Osbourn[1,9], Dinesh C. Soares[1,9], Francesco Vacca[1,9], E. Suzanne Cohen[2], Ian

4 C. Scott[2], William F. Gregory[1], Danielle J. Smyth[3,4], Matilda Toivakka[1,3], Andrea M.

5 Kemter[3,4], Thierry le Bihan[5], Martin Wear[6], Dennis Hoving[4], Kara J. Filbey[3], James

6 P. Hewitson[3,7], Holly Henderson[1], Andrea Gonzàlez-Cìscar[1,3], Claire Errington[1],

7 Sonja Vermeren[1], Anne L. Astier[1], William A. Wallace[8], Jürgen Schwarze[1],

8 Alasdair C. Ivens[3], Rick M. Maizels*[3,4,10] and Henry J. McSorley*[1,3,10]

9

10 Current Addresses

11 1. MRC Centre for Inflammation Research, University of Edinburgh, Queen's

12 Medical Research Institute, 47 Little France Crescent, Edinburgh EH16 4TJ, UK.

13 2. Department of Respiratory, Inflammation and Autoimmunity, MedImmune

14 Ltd, Granta Park, Cambridge, CB21 6GH, UK.

15 3. Institute of Immunology and Infection Research, and Centre for Immunity,

16 Infection and Evolution, School of Biological Sciences, Ashworth Laboratories,

17 University of Edinburgh, West Mains Road, Edinburgh EH9 3JT, UK.

18 4. Wellcome Centre for Molecular Parasitology, Institute for Infection, Immunity

19 and Inflammation, University of Glasgow, Sir Graeme Davies Building

20 120 University Place, Glasgow G12 8TA, UK

21 5. SynthSys, The Kings Buildings, University of Edinburgh, Edinburgh EH9 3BF,

22 UK

23 6. The Edinburgh Protein Production Facility (EPPF), Wellcome Trust Centre for

24 Cell Biology (WTCCB), University of Edinburgh, King's Buildings, Max Born

25 Crescent, Mayfield Road, Edinburgh, EH9 3BF, UK.

26   7. Centre for Immunology and Infection, Department of Biology, University of

27   York, York, UK, YO10 5DD.

28   8. Department of Pathology, Laboratory Medicine, Royal Infirmary of Edinburgh,

29   Edinburgh, UK.

30   9. These authors contributed equally

31   10. Senior author

32   * Corresponding authors henry.mcsorley@ed.ac.uk and

33   Rick.Maizels@Glasgow.ac.uk.

34   Lead contact: Dr McSorley

35

36 **Summary**

37 Infection by helminth parasites is associated with amelioration of allergic

38 reactivity, but mechanistic insights into this association are lacking. Products

39 secreted by the mouse parasite *Heligmosomoides polygyrus* suppress type 2

40 (allergic) immune responses through interference in the interleukin-33 (IL-33)

41 pathway. Here, we identified *H. polygyrus* Alarmin Release Inhibitor (HpARI), an

42 IL-33-suppressive 26-kDa protein, containing 3 predicted complement control

43 protein (CCP) modules. *In vivo*, recombinant HpARI abrogated IL-33, group 2

44 innate lymphoid cell (ILC2) and eosinophilic responses to *Alternaria* allergen

45 administration, and diminished eosinophilic responses to *Nippostrongylus*

46 *brasiliensis*, increasing parasite burden. HpARI bound directly to both mouse and

47 human IL-33 (in the cytokine's activated state), and also to nuclear DNA via its N-

48 terminal CCP module pair (CCP1/2), tethering active IL-33 within necrotic cells,

49 preventing its release, and forestalling initiation of type 2 allergic responses.

50 Thus, HpARI employs a novel molecular strategy to suppress type 2 immunity in

51 both infection and allergy.

52

53 Keywords: IL-33, helminth, parasite, allergy, asthma, immunomodulation

54

Introduction

Infection with helminth parasites negatively correlates with prevalence of allergic disease, and parasitic infection is associated with immunosuppression (Maizels and McSorley, 2016). Many researchers, ourselves included, have demonstrated that helminths release immunomodulatory proteins to control anti-parasite immune responses and maintain their persistence in the host (Maizels and McSorley, 2016). We previously showed that the excretory– secretory products of the mouse intestinal parasite *Heligmosomoides polygyrus* (HES) suppress allergic responses in mouse models of asthma (Buck et al., 2014; McSorley et al., 2015; McSorley et al., 2014; McSorley et al., 2012). HES administration blocks the interleukin-33 (IL-33) response to inhaled *Alternaria* (fungal) allergen (McSorley et al., 2014) leading to reduced type 2 innate lymphoid cell (ILC2) responses and abrogating lung pathology.

IL33 and its receptor (*IL1RL1*) are both among the 10 genes most strongly linked to allergic sensitization (Bonnelykke et al., 2013) and asthma (Bonnelykke et al., 2014; Moffatt et al., 2010) in genome-wide association studies. IL-33 concentration is increased in the lungs of severe asthmatics (Castanhinha et al., 2015; Saglani et al., 2013), correlating negatively with lung function (Christianson et al., 2015). Respiratory viral infections are implicated in both initiation and exacerbation of asthma, an effect which is also associated with IL-33 release (Jackson et al., 2014; Saravia et al., 2015).

The IL-33 receptor (ST2, IL1RL1, IL-33R) is expressed by a wide range of cells, notably T cells, macrophages, endothelial cells, epithelial cells and ILC2 (Cayrol and Girard, 2014). Through these interactions, IL-33 drives type 2 immune

79 responses in a range of diseases including asthma, atopic dermatitis, food allergy,

80 COPD, eosinophilic inflammatory bowel disease, eosinophilic esophagitis and

81 age-related macular degeneration (De Salvo et al., 2016; Liew et al., 2016; Simon

82 et al., 2015; Tordesillas et al., 2014). IL-33 is a member of the IL-1 family of

83 cytokines. It is stored preformed in the nucleus bound to heterochromatin, and

84 its dominant function is as an alarmin cytokine. Active IL-33 is released from the

85 nucleus under conditions of necrosis, while during apoptosis active caspases

86 cleave IL-33 within its receptor-binding domain, abolishing activity (Lefrancais

87 and Cayrol, 2012). Although the full-length, 30 kDa form of IL-33 is functional,

88 the activity of IL-33 is increased 10-fold through cleavage between the DNA-

89 binding and receptor-binding domains by proteases such as calpain-2 (Hristova

90 et al., 2015), neutrophil elastase, cathepsin G (Lefrancais et al., 2012) and mast

91 cell tryptase (Lefrancais et al., 2014) releasing 18-21 kDa mature forms. Active

92 IL-33 is released in a reduced form, which under physiological conditions rapidly

93 oxidizes, forming new disulfide bonds and changing conformation, rendering it

94 unable to bind to the IL-33R beyond a short temporal and spatial range (Cohen

95 et al., 2015).

96 Here, we identified *H. polygyrus* Alarmin Release Inhibitor (HpARI), a HES-

97 derived recombinant protein that can replicate the IL-33-suppressive effects of

98 total HES. HpARI bound directly to active murine and human IL-33 and nuclear

99 DNA. This dual binding blocked the interaction of IL-33 with its receptor, and

100 tethered IL-33 within necrotic cells, preventing its release, and blocking allergic

101 response initiation. Thus, HpARI prevents intuition of parasite-toxic IL-33-

102   mediated type 2 immune responses and suppresses the development of allergic

103   airway inflammation.

Results

In vitro suppression of IL-33 by HES

Previous studies established that HES ablates detectable IL-33 in the bronchoalveolar milieu after *Alternaria* allergen administration, suppressing downstream allergic responses (McSorley et al., 2014). To further investigate the IL-33-suppressive activity of HES, we developed an *in vitro* assay for IL-33 release: a single cell suspension of naïve total murine lung cells cultured for 1 h in the presence of *Alternaria* allergen and HES. In this assay, HES markedly reduced the amount of IL-33 in culture supernatants, as detected by ELISA (**Figure 1A**).

IL-33 is released from lung epithelial cells under conditions of necrosis, whereas activated caspases cleave IL-33 within the IL-1-like cytokine domain, inactivating IL-33 under conditions of apoptosis (Lefrancais and Cayrol, 2012). We therefore hypothesized that HES could be activating caspase and/or apoptosis pathways. Propidium iodide and annexin V staining showed that cells incubated with *Alternaria* allergen were highly necrotic and that this was unaffected by the presence of HES (**Figure 1B**). Necrosis induced by freeze-thaw treatment of lung cells also resulted in substantial IL-33 release, which again was abrogated by treatment of cells with HES immediately prior to freezing (**Figure 1C**). Therefore we conclude that HES suppression of IL-33 does not depend on activation of the apoptosis pathway, but instead acts on pre-formed IL-33 released from necrotic cells.

Identification and characterization of HpARI protein

A process of fractionation, screening and proteomic analysis of HES was used to identify candidate IL-33-suppressive proteins. Gel filtration and anion exchange FPLC were used to fractionate HES by size and charge, respectively. IL-33 suppressive activity peaked around size fraction 11 (**Figure 2A**) and charge fraction 25 (**Figure 2B**). Each size and charge fraction was subjected to trypsin digestion followed by liquid chromatography-electrospray tandem mass spectrometry (LC-MS/MS), and the exponentially modified protein abundance index (emPAI) value for each HES protein in every fraction was calculated, and compared to the profile of IL-33 suppression.

By size fractionation, 220 proteins were found with emPAI values which peaked around size fraction 11 (peak value in fractions 10-12), while 371 proteins were found with emPAIs which peaked around charge fraction 25 (peak value in fractions 23-27), 54 of which were shared between the two fractionation techniques. Proteins were prioritized wherein more than one peptide was detected in size fraction 11 and charge fraction 25, resulting in a short-list of 25 candidate proteins (**Supplementary Table 1**). The emPAI values for each of these 25 candidates for all size and charge fractions was then manually compared to the IL-33 suppression profile (**Supplementary Figure 1A**), and 4 candidates were selected for initial screening (**Supplementary Figure 1B**).

The 4 candidate IL-33 suppressive genes were transfected into HEK293T cells for expression, and screened for suppression of the IL-33 signal *in vitro*. Of the 4 candidates only Hp_I08176_IG02172_L1157 (candidate "D" in **Figure 2C**) significantly suppressed IL-33; this protein was consequently renamed as *H. polygyrus* Alarmin Release Inhibitor (HpARI).

151 The *HpARI* gene is made up of 7 exons, encoding a 251-aa protein including a 16-

152 aa signal peptide motif (**Supplementary Figure 2A**), with a deduced mature

153 molecular weight of 26 kDa. The mature protein contains three predicted

154 Complement Control Protein (CCP)-like modules (also known as Short

155 Consensus Repeats (SCRs) or sushi-domains, PFAM00084) (**Figure 2D**). CCP1-3

156 all contain features of a CCP module such as the four consensus Cysteine residues

157 (Cys^I to Cys^{IV}, consistent with formation of disulfide bonds in a Cys^I-Cys^{III} and

158 Cys^{II}-Cys^{IV} pattern), the Trp/Leu residue between Cys^{III} and Cys^{IV} and other

159 structurally important residues typical of a CCP module (**Figure 2D-E and**

160 **Supplementary materials and methods**)(Kirkitadze and Barlow, 2001; Soares

161 et al., 2005). Compared to archetypal CCP modules (Soares and Barlow, 2005), all

162 three are atypical in part with divergent sequence features, including an absence

163 of conserved Proline residues after Cys^I in CCP1, and atypical insertions of ~20

164 amino acid residues between Cys^I and Cys^{II} in CCP 2 and CCP3, which are unique

165 compared to previously identified CCP domains. Each CCP module is encoded by

166 two exons with the second exon boundary in each case falling between adjacent

167 predicted CCP modules (i.e. between Cys^{IV} of one module and Cys^I of the next)

168 lending further support to the discerned domain boundaries (**Figure 2E** and

169 **Supplementary Figure 2A**).

170 The three predicted HpARI CCP module sequences were modelled individually

171 based upon their top ranked CCP module template structures. Each CCP module

172 3-D model is characterised by a β-sheet framework, held together by two

173 disulfide bridges. Other key structural features such as the location of the buried

174 Trp/Leu, hypervariable loop, and potential N-glycosylation sites are indicated

175   along with the relative positions of the novel insertions in CCP2 and CCP3, which

176   could not be modelled on conventional experimentally determined CCP module

177   structures (**Figure 2F**).

178   *In vitro and in vivo IL-33 suppression by HpARI*

179   Recombinant mature 6-His and Myc-tagged HpARI protein was purified by metal

180   chelating chromatography (**Supplementary Figure 2B**), and tested for IL-33

181   suppression *in vitro*. HpARI was active at <10 ng/ml, while HES required an

182   approximately 50-fold higher concentration for a similar effect (**Figure 3A**). The

183   IL-33-suppressive activity of HpARI in response to *Alternaria* culture or freeze-

184   thaw was ablated on heat-treatment, as with HES (**Supplementary Figure 3A,**

185   **B**).

186   HpARI also effectively suppressed IL-33 detected in bronchoalveolar lavage

187   (BAL) fluids in response to *Alternaria* allergen *in vivo* (**Figure 3B**). Again this

188   effect replicated that of HES (McSorley et al., 2014) and suppression was ablated

189   when HpARI was proteolytically cleaved and heat-treated, ruling out a role for

190   non-protein contaminants. In addition, the IL-33-suppressive effects of HpARI

191   could pre-condition airway tissues, substantially reducing the IL-33 response to

192   *Alternaria* allergen 24 h later, with a degree of protection in some animals even

193   after 72 h (**Figure 3C**). Thus, HpARI appears to be a critical IL-33-suppressive

194   factor in HES.

195   *Suppression of in vivo type 2 responses by HpARI*

196   *Alternaria* exposure induces a rapid T cell-independent eosinophilia within 24 h

197   of administration. This response is driven by ILC2 cytokine release, and is

198   critically dependent on IL-33 (Bartemes et al., 2012). Recombinant HpARI co-

199   administration with *Alternaria* allergen abrogated BAL eosinophilia (**Figure 3D**)

200   and lung ILC2 IL-5 (**Figure 3E**) and IL-13 production (**Figure 3F**), 24 h later,

201   again replicating the effects observed with total HES. IL-13-eGFP reporter mice

202   were used to assess ILC2 cytokine responses in the absence of PMA and

203   Ionomycin stimulation, confirming profound suppression of IL-13 reporter

204   expression in ICOS$^+$CD90.2$^+$IL-33R$^+$CD127$^+$CD45$^+$lineage$^-$ ILC2s by HpARI

205   (**Supplementary Figure 3C-E**).

206   HpARI was administered in a T cell-dependent model of asthma, in which OVA

207   protein is first co-administered with *Alternaria*, and antigen-specific type 2

208   responses recalled 2 weeks later by challenge with OVA protein alone (McSorley

209   et al., 2014). Again HpARI replicated the suppressive effects of HES on BAL

210   eosinophilia and lung ILC2 responses (**Figure 4A-C**). Furthermore, this

211   suppression led to significantly abrogated lung resistance and compliance at

212   challenge (**Figure 4D, E**), as well as reduced inflammation and mucus production

213   assessed by histological staining (**Figure 4F-H**).

214   Finally, the role of HpARI in parasite infections was addressed using

215   *Nippostrongylus brasiliensis* infection, a parasite which (unlike *H. polygyrus*)

216   migrates through the lung and leads to early IL-33-dependent type 2 responses

217   (Hung et al., 2013). Similarly to the phenotype seen in an IL-33-deficient mouse,

218   HpARI administration did not affect worm burden at early timepoints, but

219   increased numbers of adult parasites found in the intestinal lumen at day 6

220   (**Figure 4I-J**). This suppression of parasite rejection was associated with reduced

221   BAL eosinophilia, reaching significance at day 6 (**Figure 4K**).   Thus, HpARI

222 abrogates parasite-induced, IL-33-dependent type 2 immune responses,

223 abrogating parasite ejection.

224 *HpARI binding to IL-33*

225 We hypothesised that HpARI could act by binding directly to IL-33. To

226 investigate this, we incubated Myc-tagged HpARI with murine lung cell

227 homogenates, and immunoprecipitated with anti-c-Myc antibody bound to

228 protein G-coated beads. HpARI immunoprecipitated a clear band at ~18 kDa in

229 Myc-tagged complexes eluted from anti-c-Myc-coated, but not isotype control-

230 coated beads, as revealed by anti-IL-33 Western blotting (**Figure 5A**). Unbound

231 material (supernatants from co-immunoprecipitation) showed undetectable or

232 very faint bands for IL-33 under these conditions, reflecting the manner in which

233 immunoprecipitation concentrates ligand sufficiently for detection. No band

234 could be detected for full-length IL-33 (30 kDa) in these experiments (data not

235 shown).

236 Despite human and murine IL-33 sharing only 52% amino acid identity, we

237 found that human IL-33 also co-immunoprecipitates with HpARI after incubation

238 with human lung homogenates, seen as an ~18 kDa band corresponding to

239 mature human IL-33 (**Figure 5B**). In this case, unbound human IL-33 could be

240 detected in supernatants from co-immunoprecipitation or control conditions,

241 also at ~18 kDa.

242 To biochemically characterise the binding of human and mouse IL-33 with

243 HpARI, we assessed the interactions between these proteins by surface plasmon

244 resonance (SPR) (**Figure 5C-D**). The equilibrium dissociation constant (K_d) of

245 HpARI for murine IL-33 is 0.56 ± 0.1 nM, and 260 ± 13 nM for human IL-33.

246 *Oxidation of IL-33*

247 Recently, it was shown that IL-33 is released in an active reduced form, which is

248 quickly oxidized (<4 h after release) and inactivated under physiological

249 conditions (Cohen et al., 2015). Commercially-available IL-33 ELISA kits do not

250 differentiate between the reduced and oxidized forms. Therefore we decided to

251 investigate whether HpARI preferentially bound to reduced or oxidized IL-33.

252 To attain a source of oxidized and reduced IL-33, we subjected lung cells to

253 freeze and thaw-mediated necrosis, harvested IL-33-containing supernatants

254 immediately post-thaw, and incubated these at 37°C for 1-4 h to oxidize IL-33

255 (Cohen et al., 2015). When HpARI was added to supernatants directly post-thaw,

256 or up to 2 h later, it was able to significantly reduce the IL-33 signal as measured

257 by ELISA, whereas by 4 h post-thaw, no effect of HpARI could be seen (**Figure 5E**

258 **and Supplementary Figure 4A**). Therefore we hypothesized that HpARI binds

259 only to active (reduced) IL-33.

260 HpARI co-immunoprecipitation experiments were then repeated with either

261 untreated recombinant murine IL-33 (rmIL-33) or rmIL-33 which had been

262 oxidized by incubation for 24 h at 37°C in tissue culture medium. Eluted

263 complexes were run on non-reducing SDS-PAGE gels to distinguish reduced and

264 oxidized IL-33 by their differential migration under non-reducing conditions, the

265 more compact oxidized form migrating more rapidly (Cohen et al., 2015). A

266 strong bias for binding of HpARI to the reduced form could be seen, with

267   unbound supernatants containing the oxidized form, while no unbound reduced

268   IL-33 could be detected (**Figure 5F**).

269   Co-immunoprecipitation was repeated with recombinant human IL-33 (rhIL-33),

270   either untreated or oxidized under the same conditions as applied to murine IL-

271   33. Similarly to murine IL-33, rhIL-33 could only be bound by HpARI in its

272   reduced, active form, with oxidation of IL-33 abolishing its ability to be co-

273   precipitated (**Figure 5G**).

274   Finally, we ensured that the binding of HpARI is specific to IL-33, by binding

275   studies with the closely-related IL-1 family cytokine IL-1α. No binding of HpARI

276   to IL-1α could be detected, either by co-immunoprecipitation (**Figure 5H**), or by

277   SPR (**Supplementary Figure 4B**). Thus, HpARI specifically and with high

278   affinity, binds to the active, reduced form of IL-33.

279   *HpARI prevents binding of active IL-33 to the IL-33 receptor.*

280   To investigate whether HpARI binding IL-33 consequently affected downstream

281   responses to IL-33, we investigated the binding of IL-33 to its receptor ST2.

282   Recombinant   mIL-33   was   incubated   alone   or   with   HpARI,   then

283   immunoprecipitation was carried out using an ST2-Fc fusion protein bound to

284   protein G-coated magnetic beads. The presence of HpARI completely blocked

285   immunoprecipitation of rmIL-33 by ST2-Fc (**Figure 6A**), implying that HpARI

286   prevents IL-33 from binding to its receptor.

287   Furthermore, when rmIL-33 was administered intranasally to mice, IL-33-

288   mediated ILC2 activation (measured by IL-5 and IL-13 production) was

289   effectively ablated by HpARI co-administration (**Figure 6B-C**). Thus HpARI,

290 through binding to IL-33, can prevent the activation of ILC2s through ST2

291 ligation.

292 *HpARI inhibits release of IL-33*

293 As HpARI directly binds IL-33, it could also interfere with detection of the

294 cytokine by ELISA through masking epitopes bound by assay antibodies. This

295 could affect our early screening results, (**Figures 1-3**) as these are largely

296 dependent on ELISA to measure concentrations of IL-33. To investigate the

297 possibility of undetectable HpARI-bound IL-33 in BAL supernatants, IL-33 was

298 measured by both ELISA and western blot, as the latter reduces, denatures and

299 dissociates protein complexes. Mice were treated with *Alternaria* allergen and

300 BAL taken 15 min later (at which timepoint the majority of IL-33 released is

301 active and reduced (Cohen et al., 2015)), HpARI coadministration ablated the IL-

302 33 signal by ELISA (**Figure 6D**), and significantly inhibited (but did not ablate)

303 the IL-33 signal by western blot (**Figure 6E**), implying that although HpARI

304 binding interferes with IL-33 detection by ELISA, IL-33 release is indeed

305 diminished with HpARI administration. In contrast, HpARI could not affect the

306 release of HMGB1, another nuclear-localised alarmin cytokine released on

307 necrosis, (**Supplementary Figure 4C**), demonstrating that the effects of HpARI

308 are specific to IL-33.

309 To translate these results to human biology, human lung explants were cultured

310 for 1 h with HpARI, a system and timepoint in which lung explants

311 spontaneously release reduced (active) human IL-33 (Cohen et al., 2015).

312 Similarly to the murine system, a reduction in IL-33 signal was seen with HpARI

313 coadministration, as measured by both ELISA and western blot (**Figure 6F, G**).

314 Furthermore, HpARI was administered with *Alternaria* to human IL-33

315 transgenic mice (Cohen et al., 2015), where it again suppressed human IL-33

316 release into the BAL (**Figure 6H, I**). Thus, HpARI reduces the release of both

317 mouse and human IL-33.

318 *Immunofluorescent localization of HpARI*

319 To further investigate the mechanism of action of HpARI, we utilised the CMT-64

320 mouse lung epithelial carcinoma cell line, which we found stores high amounts of

321 IL-33 in the nucleus (**Supp Figure 5A**). Similarly to lung cells cultured *in vitro*,

322 IL-33 is released from freeze-thawed CMT-64 cells, and this response is

323 suppressed by HpARI (**Supp Figure 5B**). We then produced an HpARI_mCherry

324 fusion protein, allowing fluorescent localization of HpARI binding, while

325 retaining IL-33-suppressive activity (**Supp Figure 5C**).

326 Although we found no HpARI_mCherry staining of live CMT-64 cells, binding was

327 evident in freeze-thaw treated necrotic cells (**Figure 7A**), where it bound in the

328 nucleus (**Figure 7B**). Surprisingly, we found HpARI_mCherry binds the nucleus

329 independently of IL-33 expression, as similar staining could be seen in HEK293

330 cells (**Figure 7C**), from which no IL-33 could be detected (data not shown). As

331 binding of HpARI in the nucleus of CMT-64 or HEK293 cells was ablated by

332 addition of DNAse I (**Figure 7C**), we hypothesised that HpARI binds directly to

333 DNA in the nucleus of necrotic epithelial cells.

334 *In vivo*, DNAse co-administration with *Alternaria* allergen abrogated HpARI

335 suppression of IL-33 as measured by western blot, but not by ELISA, in the latter

336 case presumably due to steric hindrance of ELISA antibodies on released HpARI-

337 bound IL-33 (**Figure 7D, E**). We conclude that dual binding of DNA and IL-33 by

338 HpARI results in retention of IL-33 within the necrotic cell nucleus, conferring a

339 tethering function on HpARI in addition to its ability to block IL-33 in the fluid

340 phase.

341 Binding of DNA by HpARI was confirmed using a gel shift assay, in which

342 addition of HpARI retarded the migration of linear plasmid DNA through an

343 agarose gel in a concentration-dependent manner (**Figure 7F**), and by

344 immunoprecipitation of plasmid DNA by HpARI (**Supp Fig 5D**). We hypothesised

345 that HpARI could bind DNA through electrostatic interactions, as shown for other

346 CCP module-containing proteins (Sjoberg et al., 2007; Trouw et al., 2005). When

347 the isoelectric point (pI) of each of the three CCP domains of HpARI were

348 calculated, CCP2 and CCP3 were found to be relatively acidic (pI 6.32 and 5.34

349 respectively), while CCP1 was strongly basic (pI 9.79). Indeed, an electrostatic

350 surface representation of our 3-D model of CCP1 (**Supp Fig 5E**), reveals clusters

351 of solvent-exposed positively charged residues that could serve as a binding site

352 for oppositely-charged (acidic) DNA. We produced truncated versions of HpARI,

353 either encoding CCP1/2 or CCP2/3. As predicted, we found that only the CCP1/2

354 truncation caused a shift in DNA migration (**Figure 7F**), supporting a role for

355 CCP1 in binding to DNA.

356 *In vivo,* only the CCP1/2 HpARI truncation could inhibit the release of IL-33 as

357 measured by western blot, while CCP2/3 actually increased total quantities of IL-

358 33 detected in the BAL (**Figure 7G**). Both constructs suppressed IL-33 detection

359 by ELISA (**Figure 7H**), indicating they could both bind IL-33 and inhibit binding

360 of ELISA antibodies. Therefore we propose that CCP2/3 does not inhibit IL-33

361   release but instead binds it in solution, prevent it from being degraded or taken

362   up via its receptor. This data supports a model by which HpARI binds to IL-33

363   through its CCP2 domain, and to DNA through its CCP1 domain, tethering IL-33

364   within the necrotic cell nucleus.

Discussion

IL-33 has emerged as a critical initiator of allergic responses in diseases such as asthma, sparking an array of type 2 reactions in innate lymphoid cells, eosinophils, macrophages and T cells (Liew et al., 2016). Through screening of the secreted products of a helminth parasite we identified HpARI, a CCP module-containing protein which inhibits IL-33 release. Recombinant HpARI is non-cell permeable, and can only gain access to the nucleus of necrotic cells, where it binds directly to IL-33 and nuclear DNA, tethering IL-33 within necrotic cells and preventing binding to the IL-33R, thereby suppressing ILC2 responses and eosinophilia in the lung after *Alternaria* administration.

The primary mechanistic effect of HpARI is to bind IL-33: remarkably this extends from murine to human IL-33. Although the affinity of HpARI for human IL-33 is lower than that of mouse IL-33, this binding is sufficient to prevent human IL-33 release, with a reduced IL-33 signal in human lung explant supernatants when cultured with HpARI, and reduced human IL-33 release in the lungs of human IL-33 transgenic mice. In the mouse, HpARI proved to be highly suppressive *in vivo*, recapitulating and exceeding the effects of total parasite secretions (HES), and able to inhibit IL-33 release even when administered 24 h prior to allergen challenge.

Although it is clear that IL-33 is released at high levels during tissue injury and necrosis, it is presently unclear how IL-33 is secreted during homeostasis (Liew et al., 2016). We showed that HpARI was not able to penetrate intact cells thus, in the absence of cell membrane damage, HpARI would be unable to mediate the nuclear retention of IL-33. HpARI's unique mechanism of action and specificity

389   provide an interesting tool to investigate the role of IL-33 as an alarmin –

390   preventing the release of IL-33 from necrotic cells while leaving other responses

391   (necrosis, HMGB1 or IL-1α release) unaffected. Recently, IL-33 production and

392   release by activated mast cells in response to extracellular ATP release was

393   demonstrated in *H. polygyrus* infection (Shimokawa et al., 2017), and

394   extracellular ATP has previously been shown to induce IL-33 release in response

395   to *Alternaria* administration (Kouzaki et al., 2011). These findings may explain

396   the lack of total ablation of IL-33 release with HpARI administration, as some

397   cytokine may be actively secreted by live mast cells, against which the tethering

398   function of HpARI would be inactive, without exposed DNA in a necrotic, lysed

399   cell. In this context, the role of *H. polygyrus* secreted apyrases (Hewitson et al.,

400   2011) - enzymes which degrade extracellular ATP – may have a further role.

401   Binding to nuclear DNA allows HpARI to hold active IL-33 within the necrotic

402   cell, and ablates allergic sensitisation. Although the affinity for DNA was not

403   determined in this study, evidence from gel shift and co-immunoprecipitation

404   assays, as well as ablation of necrotic nuclear localization and IL-33 tethering

405   function on DNAse treatment, strongly supports binding of HpARI to DNA.

406   Truncated HpARI lacking CCP1 has no activity in the gel shift assay and lack IL-

407   33 tethering functionality, and molecular modeling of CCP1 revealed 2 exposed

408   basic patches as putative DNA binding sites. Of note, the mammalian CCP

409   domain-containing proteins C4b-binding protein (C4BP) (Trouw et al., 2005) and

410   complement factor H (Leffler et al., 2010), also bind DNA through basic CCP

411   modules. The importance of IL-33 localization to the nucleus has been shown in

412   transgenic mice lacking the nuclear localization domain of IL-33, which develop

413   lethal eosinophil-dominant multi-organ inflammation (Bessa et al., 2014), and in

414   human endothelial cells, where extracellular IL-33 leads to inflammatory

415   responses, while nuclear IL-33 does not (Gautier et al., 2016).

416   Three predicted CCP modules span the length of mature HpARI. CCP module-

417   containing proteins are present in different phyla including chordates and

418   nematodes, with notable expansion and diversification in parasitic species such

419   as *H. polygyrus* (Hewitson et al., 2013). The functions of CCP modules are diverse,

420   underlining the versatility of this structural scaffold that has evolved to serve

421   many purposes (Kirkitadze and Barlow, 2001; Soares and Barlow, 2005; Soares

422   et al., 2005). Of note, no non-host CCP module-containing protein has previously

423   been shown to have immunomodulatory function outside of the complement

424   system, and hence the co-option of this module by a parasite to block a

425   mammalian immunological pathway is remarkable.

426   The suppression of the IL-33 pathway by *H. polygyrus* at the level of the IL-33

427   cytokine (mediated by HpARI) and the IL-33 receptor (mediated by secreted

428   exosomes (Buck et al., 2014)) indicates that this pathway may be critical to

429   persistence of the parasite. Indeed administration of exogenous IL-33 induces

430   expulsion of *H. polygyrus* (Yang et al., 2013), while IL-33R-deficient mice are

431   slow to expel this parasite even when immunized with a vaccine that induces

432   sterile immunity in wild-type mice (Coakley et al., 2017). Similarly, in many

433   helminth infections IL-33 administration can drive immunity, while deficiency of

434   IL-33 or the IL-33 receptor leads to increased parasite load (Maizels and

435   McSorley, 2016). Hence, the ability of *H. polygyrus* to pre-empt the IL-33 alarmin

436   system is likely to be a pivotal evolutionary adaptation to allow establishment in

437   the mammalian host.

438   HpARI administration suppressed the eosinophilic response to *N. brasiliensis*

439   infection, leading to reduced ejection of adult parasites from the intestinal

440   lumen, similarly to the phenotype seen in IL-33-deficient animals (Hung et al.,

441   2013). Thus HpARI is capable of suppressing early innate anti-parasite

442   immunity, a role we hypothesise it to play in the early stages of *H. polygyrus*

443   infection where IL-33 is critical for resistance (Shimokawa et al., 2017).

444   During an *H. polygyrus* infection, larvae penetrate the gut wall, undergo two

445   molts in the subserosal membrane, and emerge back into the lumen of the gut as

446   adults (Maizels et al., 2012). As the parasite penetrates the intestinal wall, it

447   damages epithelial cells which could result in the release of pre-formed IL-33

448   and induction of a parasite-toxic type 2 immune response. HpARI is secreted by

449   the parasite larvae and adult (Hewitson et al., 2013) and so is well positioned to

450   ablate this IL-33 response.

451   Recently, IL-33 was implicated in activation of intestinal Foxp3^{+} regulatory T

452   (Treg) cells (Schiering et al., 2014) raising the possibility that HpARI could

453   interfere with Treg cell-mediated suppression. However, in mouse models of

454   asthma, IL-33 signaling to IL-33R^{+}Foxp3^{+} Treg cells results in their expression of

455   Th2 cytokines, and abrogation of suppressive ability (Chen et al., 2017). Thus, in

456   asthmatic responses at least, IL-33 appears to have an inflammatory, rather than

457   suppressive effect.

458   In conclusion, we have identified a CCP module-containing protein with the

459   unique ability to selectively bind to IL-33 and DNA within necrotic epithelial

460   cells. This activity potently suppresses the release and the biological activity of

461   IL-33, resulting in suppression of type 2 responses to allergen challenge. IL-33 is

462   a critical mediator in allergic disease, and an important clinical target. HpARI

463   could be a potent agent for prevention of IL-33-mediated pathology, as well as a

464   new tool for manipulation of IL-33 release, leading to better understanding of the

465   IL-33 pathway.

Author Contributions:

MO, FV, ESC, ICS, WFG, MT, AMK, DJS, HH, AG, CE and HJM carried out the experiments. DCS, AMK, TB, MW and ACI carried out bioinformatic and structural analyses. AMK, KJF, JPH and HJM designed and carried out fractionation experiments. WAW provided human tissue. ESC, ICS, SV, AA, JS, RMM and HJM designed the experiments. MO, DCS, ESC, ICS, RMM and HJM wrote the manuscript.

485   **References**

486   Bartemes, K.R., Iijima, K., Kobayashi, T., Kephart, G.M., McKenzie, A.N., and Kita, H.

487   (2012). IL-33-responsive lineage- CD25+ CD44(hi) lymphoid cells mediate

488   innate type 2 immunity and allergic inflammation in the lungs. J Immunol *188*,

489   1503-1513.

490   Berman, H.M., Westbrook, J., Feng, Z., Gilliland, G., Bhat, T.N., Weissig, H.,

491   Shindyalov, I.N., and Bourne, P.E. (2000). The Protein Data Bank. Nucleic Acids

492   Res *28*, 235-242.

493   Bessa, J., Meyer, C.A., de Vera Mudry, M.C., Schlicht, S., Smith, S.H., Iglesias, A., and

494   Cote-Sierra, J. (2014). Altered subcellular localization of IL-33 leads to non-

495   resolving lethal inflammation. J Autoimmun *55*, 33-41.

496   Blein, S., Ginham, R., Uhrin, D., Smith, B.O., Soares, D.C., Veltel, S., McIlhinney, R.A.,

497   White, J.H., and Barlow, P.N. (2004). Structural analysis of the complement

498   control protein (CCP) modules of GABA(B) receptor 1a: only one of the two CCP

499   modules is compactly folded. J Biol Chem *279*, 48292-48306.

500   Bonnelykke, K., Matheson, M.C., Pers, T.H., Granell, R., Strachan, D.P., Alves, A.C.,

501   Linneberg, A., Curtin, J.A., Warrington, N.M., Standl, M.*, et al.* (2013). Meta-

502   analysis of genome-wide association studies identifies ten loci influencing

503   allergic sensitization. Nat Genet *45*, 902-906.

504   Bonnelykke, K., Sleiman, P., Nielsen, K., Kreiner-Moller, E., Mercader, J.M.,

505   Belgrave, D., den Dekker, H.T., Husby, A., Sevelsted, A., Faura-Tellez, G.*, et al.*

506 (2014). A genome-wide association study identifies CDHR3 as a susceptibility

507 locus for early childhood asthma with severe exacerbations. Nat Genet *46*, 51-55.

508 Buck, A.H., Coakley, G., Simbari, F., McSorley, H.J., Quintana, J.F., Le Bihan, T.,

509 Kumar, S., Abreu-Goodger, C., Lear, M., Harcus, Y.*, et al.* (2014). Exosomes

510 secreted by nematode parasites transfer small RNAs to mammalian cells and

511 modulate innate immunity. Nat Commun *5*, 5488.

512 Castanhinha, S., Sherburn, R., Walker, S., Gupta, A., Bossley, C.J., Buckley, J.,

513 Ullmann, N., Grychtol, R., Campbell, G., Maglione, M.*, et al.* (2015). Pediatric

514 severe asthma with fungal sensitization is mediated by steroid-resistant IL-33. J

515 Allergy Clin Immunol *136*, 312-322 e317.

516 Cayrol, C., and Girard, J.P. (2014). IL-33: an alarmin cytokine with crucial roles in

517 innate immunity, inflammation and allergy. Curr Opin Immunol *31*, 31-37.

518 Chen, C.C., Kobayashi, T., Iijima, K., Hsu, F.C., and Kita, H. (2017). IL-33

519 dysregulates regulatory T cells and impairs established immunologic tolerance

520 in the lungs. J Allergy Clin Immunol.

521 Christianson, C.A., Goplen, N.P., Zafar, I., Irvin, C., Good, J.T., Jr., Rollins, D.R.,

522 Gorentla, B., Liu, W., Gorska, M.M., Chu, H.*, et al.* (2015). Persistence of asthma

523 requires multiple feedback circuits involving type 2 innate lymphoid cells and IL-

524 33. J Allergy Clin Immunol *136*, 59-68 e14.

525 Coakley, G., McCaskill, J.L., Borger, J.G., Simbari, F., Robertson, E., Millar, M.,

526 Harcus, Y., McSorley, H.J., Maizels, R.M., and Buck, A.H. (2017). Extracellular

527   vesicles from a helminth parasite suppress macrophage activation and constitute

528   an effective vaccine for protective immunity. Cell Rep *19*, 1545-1557.

529   Cohen, E.S., Scott, I.C., Majithiya, J.B., Rapley, L., Kemp, B.P., England, E., Rees, D.G.,

530   Overed-Sayer, C.L., Woods, J., Bond, N.J.*, et al.* (2015). Oxidation of the alarmin IL-

531   33 regulates ST2-dependent inflammation. Nat Commun *6*, 8327.

532   de Castro, E., Sigrist, C.J., Gattiker, A., Bulliard, V., Langendijk-Genevaux, P.S.,

533   Gasteiger, E., Bairoch, A., and Hulo, N. (2006). ScanProsite: detection of PROSITE

534   signature matches and ProRule-associated functional and structural residues in

535   proteins. Nucleic Acids Res *34*, W362-365.

536   De Salvo, C., Wang, X.M., Pastorelli, L., Mattioli, B., Omenetti, S., Buela, K.A.,

537   Chowdhry, S., Garg, R.R., Goodman, W.A., Rodriguez-Palacios, A.*, et al.* (2016). IL-

538   33 Drives Eosinophil Infiltration and Pathogenic Type 2 Helper T-Cell Immune

539   Responses Leading to Chronic Experimental Ileitis. Am J Pathol.

540   Gautier, V., Cayrol, C., Farache, D., Roga, S., Monsarrat, B., Burlet-Schiltz, O.,

541   Gonzalez de Peredo, A., and Girard, J.P. (2016). Extracellular IL-33 cytokine, but

542   not endogenous nuclear IL-33, regulates protein expression in endothelial cells.

543   Sci Rep *6*, 34255.

544   Hewitson, J.P., Harcus, Y., Murray, J., van Agtmaal, M., Filbey, K.J., Grainger, J.R.,

545   Bridgett, S., Blaxter, M.L., Ashton, P.D., Ashford, D.A.*, et al.* (2011). Proteomic

546   analysis of secretory products from the model gastrointestinal nematode

547   *Heligmosomoides polygyrus* reveals dominance of venom allergen-like (VAL)

548   proteins. J Proteomics *74*, 1573-1594.

549   Hewitson, J.P., Ivens, A.C., Harcus, Y., Filbey, K.J., McSorley, H.J., Murray, J.,

550   Bridgett, S., Ashford, D., Dowle, A.A., and Maizels, R.M. (2013). Secretion of

551   protective antigens by tissue-stage nematode larvae revealed by proteomic

552   analysis and vaccination-induced sterile immunity. PLoS Pathog *9*, e1003492.

553   Howe, K.L., Bolt, B.J., Cain, S., Chan, J., Chen, W.J., Davis, P., Done, J., Down, T., Gao,

554   S., Grove, C.*, et al.* (2016). WormBase 2016: expanding to enable helminth

555   genomic research. Nucleic Acids Res *44*, D774-780.

556   Hristova, M., Habibovic, A., Veith, C., Janssen-Heininger, Y.M., Dixon, A.E., Geiszt,

557   M., and van der Vliet, A. (2016). Airway epithelial dual oxidase 1 mediates

558   allergen-induced IL-33 secretion and activation of type 2 immune responses. J

559   Allergy Clin Immunol *137,* 1545-1556

560   Hung, L.Y., Lewkowich, I.P., Dawson, L.A., Downey, J., Yang, Y., Smith, D.E., and

561   Herbert, D.R. (2013). IL-33 drives biphasic IL-13 production for noncanonical

562   Type 2 immunity against hookworms. Proc Natl Acad Sci U S A *110*, 282-287.

563   Jackson, D.J., Makrinioti, H., Rana, B.M., Shamji, B.W., Trujillo-Torralbo, M.B.,

564   Footitt, J., Jerico, D.-R., Telcian, A.G., Nikonova, A., Zhu, J.*, et al.* (2014). IL-33-

565   dependent type 2 inflammation during rhinovirus-induced asthma exacerbations

566   in vivo. Am J Respir Crit Care Med *190*, 1373-1382.

567   Johnston, C.J., Robertson, E., Harcus, Y., Grainger, J.R., Coakley, G., Smyth, D.J.,

568   McSorley, H.J., and Maizels, R. (2015). Cultivation of *Heligmosomoides polygyrus*:

569   an immunomodulatory nematode parasite and its secreted products. J Vis Exp,

570   e52412.

571 Jordan, M., Schallhorn, A., and Wurm, F.M. (1996). Transfecting mammalian cells:

572 optimization of critical parameters affecting calcium-phosphate precipitate

573 formation. Nucleic Acids Res *24*, 596-601.

574 Kirkitadze, M.D., and Barlow, P.N. (2001). Structure and flexibility of the multiple

575 domain proteins that regulate complement activation. Immunol Rev *180*, 146-

576 161.

577 Kouzaki, H., Iijima, K., Kobayashi, T., O'Grady, S.M., and Kita, H. (2011). The

578 danger signal, extracellular ATP, is a sensor for an airborne allergen and triggers

579 IL-33 release and innate Th2-type responses. J Immunol *186*, 4375-4387.

580 Lawrence, R.A., Gray, C.A., Osborne, J., and Maizels, R.M. (1996). *Nippostrongylus*

581 *brasiliensis*: cytokine responses and nematode expulsion in normal and IL-4-

582 deficient mice. Exp Parasitol *84*, 65-73.

583 Leffler, J., Herbert, A.P., Norstrom, E., Schmidt, C.Q., Barlow, P.N., Blom, A.M., and

584 Martin, M. (2010). Annexin-II, DNA, and histones serve as factor H ligands on the

585 surface of apoptotic cells. J Biol Chem *285*, 3766-3776.

586 Lefrancais, E., and Cayrol, C. (2012). Mechanisms of IL-33 processing and

587 secretion: differences and similarities between IL-1 family members. Eur

588 Cytokine Netw *23*, 120-127.

589 Lefrancais, E., Duval, A., Mirey, E., Roga, S., Espinosa, E., Cayrol, C., and Girard, J.P.

590 (2014). Central domain of IL-33 is cleaved by mast cell proteases for potent

591 activation of group-2 innate lymphoid cells. Proc Natl Acad Sci U S A *111*, 15502-

592 15507.

593 Lefrancais, E., Roga, S., Gautier, V., Gonzalez-de-Peredo, A., Monsarrat, B., Girard,

594 J.P., and Cayrol, C. (2012). IL-33 is processed into mature bioactive forms by

595 neutrophil elastase and cathepsin G. Proc Natl Acad Sci U S A *109*, 1673-1678.

596 Letunic, I., Doerks, T., and Bork, P. (2015). SMART: recent updates, new

597 developments and status in 2015. Nucleic Acids Res *43*, D257-260.

598 Liew, F.Y., Girard, J.P., and Turnquist, H.R. (2016). Interleukin-33 in health and

599 disease. Nat Rev Immunol *16*, 676-689.

600 Lovell, S.C., Davis, I.W., Arendall, W.B., 3rd, de Bakker, P.I., Word, J.M., Prisant,

601 M.G., Richardson, J.S., and Richardson, D.C. (2003). Structure validation by Calpha

602 geometry: phi,psi and Cbeta deviation. Proteins *50*, 437-450.

603 Maizels, R.M., Hewitson, J.P., Murray, J., Harcus, Y.M., Dayer, B., Filbey, K.J.,

604 Grainger, J.R., McSorley, H.J., Reynolds, L.A., and Smith, K.A. (2012). Immune

605 modulation and modulators in *Heligmosomoides polygyrus* infection. Exp

606 Parasitol *132*, 76-89.

607 Maizels, R.M., and McSorley, H.J. (2016). Regulation of the host immune system

608 by helminth parasites. J Allergy Clin Immunol *138*, 666-675.

609 Makou, E., Mertens, H.D., Maciejewski, M., Soares, D.C., Matis, I., Schmidt, C.Q.,

610 Herbert, A.P., Svergun, D.I., and Barlow, P.N. (2012). Solution structure of CCP

611 modules 10-12 illuminates functional architecture of the complement regulator,

612 factor H. J Mol Biol *424*, 295-312.

613 McSorley, H.J., Blair, N.F., Robertson, E., and Maizels, R.M. (2015). Suppression of

614 OVA-alum induced allergy by *Heligmosomoides polygyrus* products is MyD88-,

615   TRIF-, regulatory T- and B cell-independent, but is associated with reduced

616   innate lymphoid cell activation. Exp Parasitol *158*, 8-17.

617   McSorley, H.J., Blair, N.F., Smith, K.A., McKenzie, A.N., and Maizels, R.M. (2014).

618   Blockade of IL-33 release and suppression of type 2 innate lymphoid cell

619   responses by helminth secreted products in airway allergy. Mucosal Immunol *7*,

620   1068-1078.

621   McSorley, H.J., O'Gorman, M.T., Blair, N., Sutherland, T.E., Filbey, K.J., and Maizels,

622   R.M. (2012). Suppression of type 2 immunity and allergic airway inflammation

623   by secreted products of the helminth *Heligmosomoides polygyrus*. Eur J Immunol

624   *42*, 2667-2682.

625   Moffatt, M.F., Gut, I.G., Demenais, F., Strachan, D.P., Bouzigon, E., Heath, S., von

626   Mutius, E., Farrall, M., Lathrop, M., Cookson, W.O., and Consortium, G. (2010). A

627   large-scale, consortium-based genomewide association study of asthma. N Engl J

628   Med *363*, 1211-1221.

629   Morgan, H.P., Mertens, H.D., Guariento, M., Schmidt, C.Q., Soares, D.C., Svergun,

630   D.I., Herbert, A.P., Barlow, P.N., and Hannan, J.P. (2012). Structural analysis of the

631   C-terminal region (modules 18-20) of complement regulator factor H (FH). PLoS

632   One *7*, e32187.

633   Neill, D.R., Wong, S.H., Bellosi, A., Flynn, R.J., Daly, M., Langford, T.K., Bucks, C.,

634   Kane, C.M., Fallon, P.G., Pannell, R*., et al.* (2010). Nuocytes represent a new innate

635   effector leukocyte that mediates type-2 immunity. Nature *464*, 1367-1370.

636   Prota, A.E., Sage, D.R., Stehle, T., and Fingeroth, J.D. (2002). The crystal structure

637   of human CD21: Implications for Epstein-Barr virus and C3d binding. Proc Natl

638   Acad Sci U S A *99*, 10641-10646.

639   Robert, X., and Gouet, P. (2014). Deciphering key features in protein structures

640   with the new ENDscript server. Nucleic Acids Res *42*, W320-324.

641   Saglani, S., Lui, S., Ullmann, N., Campbell, G.A., Sherburn, R.T., Mathie, S.A.,

642   Denney, L., Bossley, C.J., Oates, T., Walker, S.A.*, et al.* (2013). IL-33 promotes

643   airway remodeling in pediatric patients with severe steroid-resistant asthma. J

644   Allergy Clin Immunol *132*, 676-685 e613.

645   Sali, A., and Blundell, T.L. (1993). Comparative protein modelling by satisfaction

646   of spatial restraints. J Mol Biol *234*, 779-815.

647   Saravia, J., You, D., Shrestha, B., Jaligama, S., Siefker, D., Lee, G.I., Harding, J.N.,

648   Jones, T.L., Rovnaghi, C., Bagga, B.*, et al.* (2015). Respiratory Syncytial Virus

649   Disease Is Mediated by Age-Variable IL-33. PLoS Pathog *11*, e1005217.

650   Schiering, C., Krausgruber, T., Chomka, A., Frohlich, A., Adelmann, K., Wohlfert,

651   E.A., Pott, J., Griseri, T., Bollrath, J., Hegazy, A.N.*, et al.* (2014). The alarmin IL-33

652   promotes regulatory T-cell function in the intestine. Nature *513*, 564-568.

653   Shen, M.Y., and Sali, A. (2006). Statistical potential for assessment and prediction

654   of protein structures. Protein Sci *15*, 2507-2524.

655   Shimokawa, C., Kanaya, T., Hachisuka, M., Ishiwata, K., Hisaeda, H., Kurashima, Y.,

656   Kiyono, H., Yoshimoto, T., Kaisho, T., and Ohno, H. (2017). Mast Cells Are Crucial

657   for Induction of Group 2 Innate Lymphoid Cells and Clearance of Helminth

658   Infections. Immunity *46*, 863-874 e864.

659   Simon, D., Radonjic-Hosli, S., Straumann, A., Yousefi, S., and Simon, H.U. (2015).

660   Active eosinophilic esophagitis is characterized by epithelial barrier defects and

661   eosinophil extracellular trap formation. Allergy *70*, 443-452.

662   Sjoberg, A.P., Trouw, L.A., Clark, S.J., Sjolander, J., Heinegard, D., Sim, R.B., Day,

663   A.J., and Blom, A.M. (2007). The factor H variant associated with age-related

664   macular degeneration (His-384) and the non-disease-associated form bind

665   differentially to C-reactive protein, fibromodulin, DNA, and necrotic cells. J Biol

666   Chem *282*, 10894-10900.

667   Soares, D.C., and Barlow, P.N. (2005). Complement Control Protein Modules in

668   the Regulators of Complement Activation. In Structural Biology of the

669   Complement System, D. Morikis, and J.D. Lambris, eds. (Boca Raton: Taylor &

670   Francis), pp. 19-62.

671   Soares, D.C., Gerloff, D.L., Syme, N.R., Coulson, A.F., Parkinson, J., and Barlow, P.N.

672   (2005). Large-scale modelling as a route to multiple surface comparisons of the

673   CCP module family. Protein Eng Des Sel *18*, 379-388.

674   Soding, J. (2005). Protein homology detection by HMM-HMM comparison.

675   Bioinformatics *21*, 951-960.

676   Thompson, J.D., Gibson, T.J., Plewniak, F., Jeanmougin, F., and Higgins, D.G.

677   (1997). The CLUSTAL_X windows interface: flexible strategies for multiple

678   sequence alignment aided by quality analysis tools. Nucleic Acids Res *25*, 4876-

679   4882.

680   Tordesillas, L., Goswami, R., Benede, S., Grishina, G., Dunkin, D., Jarvinen, K.M.,

681   Maleki, S.J., Sampson, H.A., and Berin, M.C. (2014). Skin exposure promotes a

682   Th2-dependent sensitization to peanut allergens. J Clin Invest *124*, 4965-4975.

683   Trouw, L.A., Nilsson, S.C., Goncalves, I., Landberg, G., and Blom, A.M. (2005). C4b-

684   binding protein binds to necrotic cells and DNA, limiting DNA release and

685   inhibiting complement activation. J Exp Med *201*, 1937-1948.

686   Yang, Z., Grinchuk, V., Urban, J.F., Jr., Bohl, J., Sun, R., Notari, L., Yan, S.,

687   Ramalingam, T., Keegan, A.D., Wynn, T.A.*, et al.* (2013). Macrophages as IL-25/IL-

688   33-responsive cells play an important role in the induction of type 2 immunity.

689   PLoS One *8*, e59441.

690

691
692

693   **Figure Legends**

694   **Figure 1: HES suppression of IL-33**

695   (A)   IL-33 levels (ELISA) in supernatants of naive murine lung cells (1×10^5 per

696   well), cultured for 1 h with *Alternaria* (Alt) allergen (200 µg/ml) and HES

697   (10 µg/ml).

698   (B)   Propidium iodide (PI) and annexin V (AnnV) staining of cells from (A) was

699   used to assess apoptosis (PI–AnnV+) versus necrosis (PI+AnnV+).

700   (C)   IL-33 levels (ELISA) in supernatants of naive murine lung cells, freeze-

701   thawed in the presence of HES.

702   All data shows SEM of 2-3 replicates, and are representative of 2-3 repeat

703   experiments.

704

Figure 2: Identification and bioinformatic characterization of HpARI

sequence and structure

(A)   IL-33 suppression by HES size fractions.

(B)   IL-33 suppression by HES charge fractions.

Data in (A) and (B) are percentage suppression of the IL-33 signal compared to *Alternaria*-only control. Dotted rectangles indicate peaks used for selection of candidates.

(C)   IL-33 levels (ELISA) in supernatants of naïve murine lung cells, freeze-thawed in the presence of supernatants of HEK293T cells transfected with four candidate genes. Mean and SEM are shown of 3 replicate wells, representative of 3 repeat experiments.

(D)   Alignment of HpARI CCP-like modules with complement receptor type 2 CCP2 (CR2-CCP2) and complement factor H CCP10 (FH-CCP10). The putative disulfide bonding pattern (C^I-C^{III}; C^{II}-C^{IV}), conserved tryptophan (W) and structurally-important proline (P), glycine (G) and hydrophobic amino acid residues (h), characteristic of a CCP-module are indicated. Atypical insertions in CCP2/3 (green box), the hypervariable loop (cyan box) and beta-strands (pink arrows) are indicated, based on known CCP secondary structure of CR2-CCP2, as well as three potential N-linked glycosylation sites (light green box).

(E)   HpARI domain schematic, with putative disulfide bonding pattern and location of insertions indicated.

(F)   Structural models of the three HpARI CCP-like modules.

Figure 3: HpARI suppresses responses to *Alternaria* allergen

(A) IL-33 levels (ELISA) in supernatants of naive mouse lung cells, cultured for 1 h in the presence of *Alternaria* (200 µg/ml) and HES or HpARI.

(B) IL-33 levels (ELISA) in BAL 1h after *Alternaria* allergen administration with HpARI (5 µg) or proteinase K-degraded and heat-treated HpARI ("HpARI (prK)").

(C) IL-33 levels (ELISA) in BAL 1 h after *Alternaria* allergen administration, with HpARI (5 µg) administered 1, 24, 72 or 168 h prior to *Alternaria* allergen.

(D) BAL eosinophil numbers 24 h after *Alternaria* allergen, HpARI and HES administration.

(E) Lung ILC2 IL-5 staining from mice in (D).

(F) Lung ILC2 IL-13 staining from mice in (D).

All data representative of 2-3 repeat experiments, each with 3-4 replicates/mice per group.

Figure 4: HpARI suppresses responses to *Alternaria* allergen

(A) Day 17 BAL eosinophil numbers after *Alternaria* allergen, OVA protein

and HpARI administeration on day 0 (sensitisation), and OVA protein

alone on days 14, 15 and 16 (challenge).

(B) Lung ILC2 IL-5 production from mice in (A).

(C) Lung ILC2 IL-13 production from mice in (A)

(D) Lung resistance in methacholine challenge from mice treated as in (A)

(E) Lung compliance in methacholine challenge from mice treated as in

(A)

(F) H&E- (top panels) and PAS-stained (bottom panels) lung sections

from mice treated as in (A). Scale bars indicate 100 μm.

(G) H&E scoring of sections from mice treated as in (A).

(H) PAS scoring of sections from mice treated as in (A)

Alternaria model data representative of 2-3 repeat experiments, each with 4-

6 mice per group.

(I) Mice were subcutaneously infected with *N. brasiliensis*, and HpARI

administered intranasally on days 0, 1 and 2 of infection. Lung larvae

were counted 3 days after infection.

(J) Day 6 intestinal *N. brasiliensis* worms from mice treated as in (I).

(K) Day 3 and day 6 BAL eosinophil numbers from mice treated as in (I).

766 **Figure 5: HpARI binds active murine and human IL-33**

767 (A) Murine IL-33 western blot (non-reducing) of HpARI immunoprecipitation

768 of mouse lung homogenates, using anti-c-Myc antibody, or MOPC isotype

769 control (iso).

770 (B) Human IL-33 western blot (non-reducing) of HpARI immunoprecipitation

771 of human lung homogenates, as in (A).

772 (C) Characterization of the interaction of mouse IL-33 (mIL-33) with HpARI by

773 surface plasmon resonance (SPR - BIAcore T200). Reference corrected single

774 kinetic titration SPR binding curves (black), and a globally fitted 1:1 kinetic

775 binding model (grey).

776 (D) Characterisation by SPR of the interaction of human IL-33 (hIL-33) with

777 HpARI, as in (C).

778 (E) IL-33 levels (ELISA) in supernatants of freeze-thawed murine lung cells,

779 incubated at 37°C for 0, 1, 2 or 4 h, before addition of 1 μg/ml HpARI, and a

780 further incubation for 1 h at 37°C.

781 (F) Untreated or oxidised recombinant murine IL-33 immunoprecipitated with

782 HpARI as in (A).

783 (G) Untreated or oxidised recombinant human IL-33 immunoprecipitated with

784 HpARI as in (B)

785 (H) Immunoprecipitation experiments repeated with recombinant murine IL-

786 1α, and probed with anti-murine IL-1α.

787 Arrows indicate specific IL-33 or IL-1α bands, and IL-33 reduced ("red") or

788 oxidised ("ox") bands. All data representative of at least 2 independent repeats.

Figure 6: HpARI blocks IL-33-ST2 interactions and inhibits IL-33 release

790 (A) IL-33 western blot (non-reducing) of ST2-Fc fusion protein

791   immunoprecipitation of recombinant murine IL-33 in the presence or

792   absence of HpARI.

793 (B) Lung ILC2 IL-5 production 24 h after intranasal administration of

794   recombinant murine IL-33 (200 ng/mouse) with 5 µg HpARI.

795 (C) Lung ILC2 IL-5 production from mice described in (B).

796 (D) Murine IL-33 levels (ELISA) in BAL 15 min after *Alternaria* allergen and

797   HpARI were intranasally administered.

798 (E) Murine IL-33 western blot (~20 kDa band and densitometry analysis) of

799   BAL from mice described in (D).

800 (F) Human IL-33 levels (ELISA) in supernatants of human lung explants

801   cultured for 1 h with HpARI.

802 (G) Human IL-33 western blot (~20 kDa band and densitometry analysis) of

803   supernatants from human lung explants cultures described in (F).

804 (H) Human IL-33 levels (ELISA) in BAL fluid of human IL-33-transgenic mice,

805   30 min after *Alternaria* allergen and HpARI intranasally administration.

806 (I) Human IL-33 western blot (~20 kDa band and densitometry analysis) of

807   BAL from human IL-33-transgenic mice described in (H).

808 Mouse data (A-E, H-I) representative of 2-4 repeat experiments, each with 3-4

809 mice per group. Human data (C, D) shows 5 independent subjects.

Figure 7: HpARI binds nuclear DNA, tethering IL-33 within necrotic cells

(A)   Live (top panels) or freeze-thawed (bottom panels) CMT-64 cells were incubated for 1 h at 37°C with 5 μg/ml HpARI_mCherry.

(B)   HpARI_mCherry-stained freeze-thawed CMT-64 cells, with Hoechst 33342 nuclear co-stain.

(C)   Freeze-thawed CMT-64 or HEK293T cells were stained with HpARI_mCherry with 100 U/ml DNAse I.

(D)   Murine IL-33 western blot densitometry of BAL taken 15 min after *Alternaria* allergen, HpARI and DNAse (100 U) intranasal administration.

(E)   Murine IL-33 levels (ELISA) IL-33 in BAL fluid from mice described in (D)

(F)   Gel shift assay of linearised plasmid DNA, incubated with 100, 50 or 25 pmol of HpARI, CCP1/2 or CCP2/3 truncated proteins..

(G)   Murine IL-33 western blot densitometry of BAL taken 15 min after *Alternaria* allergen, HpARI or CCP1/2 or CCP2/3 HpARI truncated proteins intranasal administration.

(H)   Murine IL-33 levels (ELISA) in BAL from mice described in (G).

All data representative of at least 2 repeat experiments. Data in (D) and (E) shows mean and SEM of 3 pooled experiments, data log-transformed for statistical analysis to equalize variances. Scale bars = 100 μm.

830 **CONTACT FOR REAGENT AND RESOURCE SHARING**

831 **Further information and request for resources and reagents should be**

832 **directed to and will be fulfilled by the Lead Contact, Henry McSorley**

833 **(henry.mcsorley@ed.ac.uk).**

834

835 **EXPERIMENTAL MODEL AND SUBJECT DETAILS**

836 *Mice*

837 BALB/cOlaHsd, C57BL/6JOlaHsd, IL-13-eGFP (C57BL/6 background) (Neill et al.,

838 2010) and ST2-deficient (BALB/c background, kindly provided by Dr Andrew

839 McKenzie, MRC Laboratory of Molecular Biology, Cambridge) mice, male or

840 female (single sex within an experiment), 6-10 weeks old, were bred in-house at

841 the University of Edinburgh. hIL-33$^{+/+}$, mIL-33$^{-/-}$ (humanised IL-33) transgenic

842 mice (BALB/c background) (Cohen et al., 2015) were bred in-house at the

843 Babraham Institute, Cambridge. All mice were accommodated, and procedures

844 performed under UK Home Office licenses with institutional oversight performed

845 by qualified veterinarians.

846 *Human Tissue Samples*

847 Non-cancerous adjacent tissue from lung cancer patients was collected by

848 Lothian NRS Bioresource, and cultured as previously described (Cohen et al.,

849 2015). The study was approved by Lothian NRS Bioresource (15/ES/0094) and

850 tissue was donated with the informed consent of patients.

851

852 **METHOD DETAILS**

853 *Parasite lifecycles, infection and HES preparation*

854   The life cycle of *H. polygyrus bakeri* was maintained, and HES products prepared,

855   as previously described (Johnston et al., 2015). The life cycle of *N. brasiliensis*

856   was maintained in Sprague-Dawley rats as previously described (Lawrence et al.,

857   1996), and infective L3 larvae were prepared from 1-3 week rat fecal cultures.

858   BALB/c mice were subcutaneously infected with 500 L3 *N. brasiliensis* larvae. At

859   day 3 post-infection, larvae were counted in the bronchoalveolar lavage and in

860   lung tissue, by dicing lungs and placing them in a cheese-cloth bag in a 50 ml

861   tube containing PBS at 37°C for at least 3 h. Day 3 lung counts reflect a sum of the

862   BAL and lung larval counts for each animal. At day 6 intestinal worms were

863   recovered from intestinal tissue using an adapted Baermann apparatus.

864

865   ***Reagents*:**

866   *Alternaria alternata* extract (Greer XPM1D3A25) was resuspended in PBS, filter

867   sterilized and concentration assessed by BCA assay (Pierce). CMT-64 cells

868   (ECACC 10032301) and HEK293T cells (ATCC CRL-3216) were maintained by

869   serial passage in DMEM medium containing 10% fetal bovine serum, 2 mM L-

870   glutamine and 1 μ g ml^{-1} penicillin/streptomycin. Human and murine IL-33 and

871   murine IL-1α were purchased from BioLegend.

872   ***In vitro IL-33 release assay:***

873   HES, candidate proteins or HpARI were cultured with total murine lung cells

874   prepared by Liberase/DNAse digestion of naïve mouse lungs or CMT-64 cells for

875   1 h at 37°C, 5% CO$_2$, with *Alternaria* allergen (200 µg ml^{-1}), or were frozen on dry

876   ice, and thawed at 37°C.

877   ***Preparation of murine lung single cell suspension:***

878   Single-cell suspensions of naïve murine lung tissue were prepared by digesting

879   in 2 U ml^{-1} liberase TL (Roche, Burgess Hill, UK) and 80 U ml^{-1} DNase (Life

880   Technologies, Paisley, UK) at 37°C with agitation for 35 min. Digested tissue was

881   macerated through a 70 μm cell strainer (BD Biosciences), treated with red

882   blood cells lysis buffer (Sigma), and live cells counted on a haemocytometer,

883   excluding dead cells by trypan blue staining.

884   ***Cytokine measurement:***

885   R&D Systems Duoset kits were used to measure human and murine IL-33 by

886   ELISA, while western blotting was carried out using polyclonal goat anti-mouse

887   IL-33, goat anti-human IL-33 or goat anti-mouse IL-1α (R&D Systems) with a

888   rabbit anti-goat IgG HRP secondary antibody (Thermo Fisher), and detected

889   using WesternSure Premium reagent (Licor).

890   ***Fractionation and mass spectrometry:***

891   HES was separated into 1 ml fractions by size exclusion chromatography using a

892   Superdex 200 10/300 GL column, or by anion exchange chromatography using a

893   MonoQ 5/50 GL column (GE Healthcare) in a 40 column volume gradient from

894   20 mM TrisHCl pH 8 (start buffer) to a maximum of 30 % 20 mM TrisHCl + 1 M

895   NaCl pH 8 (elution buffer). All fractions were trypsinized and analyzed by LC

896   MS/MS on an on-line system consisting of a capillary-pump Agilent 1200 HPLC

897   system (Agilent, UK) coupled to an Orbitrap XL mass spectrometer (Thermo

898   Scientific) as previously described (Hewitson et al., 2011; Hewitson et al., 2013).

899   LC MS/MS data was analyzed using Mascot (v2.4, Matrix Science) and searched

900   against an improved in-house BLASTx annotated database obtained by 454

901   sequencing of *H. polygyrus* adults, with additional full length *H. polygyrus*

902   sequences from NCBI, WormBase ParaSite (Howe et al., 2016) and our own

903 Sanger sequencing (Harcus Y. et al, manuscript in preparation). Peptides

904 identified were ranked by Mascot protein score, with a minimum cutoff score of

905 20, with a significance threshold of $p < 0.05$. Protein abundance was estimated by

906 emPAI (exponentially modified protein abundance index).

907 ***Protein expression and purification***

908 Candidate genes were selected by comparison of emPAI and IL-33-suppression

909 profiles in all fractions (**Supplementary Figures 1-2**). Candidate genes A-D

910 (**Figure 2A**, respectively Hp_I10793_IG03481_L623, Hp_I15874_IG07818_L1106,

911 Hp_I46029_IG37973_L313 and Hp_I08176_IG02172_L1157 transcripts) were

912 codon optimised for *Homo sapiens* and gene synthesised (GeneArt, Thermo

913 Fisher) with 5' AscI and 3' NotI restriction enzyme sites. CCP1/2 (amino acids

914 17-165) and CCP2/3 (amino acids 80-251) constructs were created using PCR of

915 codon-optimised HpARI, and primers which added a NotI site 3' of the CCP2

916 module (5'GCGGCCGCCTTGGGGCACACGCCCAG3', primes reverse of LGVCPK

917 amino acid sequence, for CCP1/2 construct), or an AscI site 5' of the CCP2

918 module (5' 5'GGCGCGCCGGCTGCAAGGGCATCCTG3', primes GCKGIL amino acid

919 sequence, for CCP2/3 construct), combined with vector-specific T7 (5' of insert)

920 and BGH (3' of insert) primers. The HpARI_mCherry fusion protein was created

921 by cloning in a codon-optimised gene-synthesised mCherry sequence

922 (ANO45948.1) at the C-terminus of the HpARI protein, using an mCherry 5' NotI

923 site and a 3' ApaI site. These constructs were sub-cloned into the pSecTAG2A

924 expression vector (Thermo Fisher), using AscI, NotI-HF and Apa-1 restriction

925 enzyme digestion (New England Biolabs), followed by T4 DNA ligation (Thermo

926 Fisher).

927   JM109 cells were transformed with ligated constructs and plasmids were

928   midiprepped using the PureLink HiPure midiprep kit (Thermo Fisher) according

929   to manufacturers instructions, and Sanger sequenced. Plasmid constructs were

930   transfected into HEK293T cells using the calcium phosphate technique (Jordan et

931   al., 1996), using 15 μg plasmid DNA per 100 mm tissue culture dish of HEK293T

932   cells at 20% confluency. Stable cell lines were maintained using Zeocin (Thermo

933   Fisher) selection in DMEM medium containing 10% fetal bovine serum, 2 mM L-

934   glutamine and 1 μg ml^{-1} Penicillin/Streptomycin.

935   Resulting expressed proteins secreted to the medium contained C-terminal myc

936   and 6-His tags. For large scale expression of constructs, transfected cells were

937   transferred to 293 SFM II media (Thermo Fisher) and protein purified from

938   supernatant by nickel affinity chromatography using HiTrap chelating HP

939   columns (GE Healthcare), eluting bound proteins using an imidazole gradient.

940   Fractions containing pure expressed protein were pooled, dialysed into PBS,

941   sterile filtered and concentration assessed by absorbance at 280 nm, corrected

942   by calculated extinction coefficient.

943   Purified HpARI had an endotoxin content of below 0.5 U LPS per μg protein, as

944   measured by the Limulus Amoebocyte Lysate assay (Lonza).

945   ***Bioinformatics characterization and modeling:***

946   Domain identification and assignment were undertaken using a combination of

947   SMART (Letunic et al., 2015), an HHPred search against the pdb70 database

948   (accessed March 2016) (Berman et al., 2000; Soding, 2005), and refined

949   manually based upon positioning of the four Cysteine residues that typify CCP

950   module sequences (Soares et al., 2005). PROSITE (de Castro et al., 2006) was

951   used for short motif searches. ESPript v3 (Robert and Gouet, 2014) was used for

952   alignment figure preparation.

953   The three predicted HpARI CCP module sequences were modeled based upon

954   their top ranked CCP module template structure 'hits' as suggested by HHPred.

955   HpARI-CCP1 was modeled based upon CR2-CCP2 (PDB ID: 1LY2) (Prota et al.,

956   2002) (after a manual switch of Leu[69] with Trp[69] to help identify this CCP module

957   using HHPred; note Leu/Trp substitutions exist in other experimentally-

958   determined CCP module structures such as complement Factor H CCP10 and

959   CCP20 (Makou et al., 2012; Morgan et al., 2012); HpARI-CCP2 on CSMD1-CCP3

960   (PDB ID: 2EHF) (RIKEN Structural Genomics/Proteomics Initiative); HpARI-

961   CCP3 on GABABR1α-CCP2 (PDB ID: 1SRZ) (Blein et al., 2004). The target-

962   template alignment in each case was based upon the initial HHPred alignment,

963   then extended to include the first Cysteine residue in each domain, realigned

964   using ClustalX (Thompson et al., 1997), and finally subjected to manual editing to

965   optimally position known consensus residues, secondary structure elements and

966   gaps (Soares et al., 2005). Note, an alternative alignment for the atypical

967   insertion in CCP3 is possible where it can be accommodated after the

968   hypervariable loop (not shown). A total of 100 models for each CCP module were

969   built using Modeller v9.12 (Sali and Blundell, 1993), and the model with the

970   lowest DOPE (Shen and Sali, 2006) energy score selected as the representative

971   model in each case and evaluated for valid stereochemistry (Lovell et al., 2003).

972   Electrostatic surface potential was calculated using APBS (Baker et al, 2001).

973   PyMOL (http://www.pymol.org/; Schrödinger, LLC.) was used for visualization,

974   and figure preparation.

975   ***Alternaria models***

976 *Alternaria* models, lung cell preparation, flow cytometry and lung histology were

977 carried out as previously described (McSorley et al., 2014). *Alternaria* allergen

978 (25 μg) was administered intranasally with 20 μg OVA protein (Sigma) and

979 HpARI (10 μg). In some experiments, the OVA-specific response was recalled by

980 daily intranasal administration of 20 μg OVA protein on days 14, 15 and 16. Mice

981 were culled 15 min, 1 h, 24 h or 17 days after the initial administration, as

982 indicated. Bronchoalveloar lavage was collected (4 lavages with 0.5 ml ice-cold

983 PBS), followed by lung dissection for tissue digestion and single cell preparation

984 (see below), or lungs were inflated with 10% neutral buffered formalin for

985 histology. Formalin-fixed lungs were transferred into 70% ethanol 24 h after

986 collection, paraffin, embedded and sectioned (5 μm), prior to staining with

987 haemotoxylin and eosin (H&E) or Periodic Acid Schiff (PAS). H&E and PAS-

988 stained sections were scored blindly according to the following criteria: H&E

989 stain at 200X magnification on an increasing severity score of 1–4 in both the

990 peri-vascular and peri-bronchiolar compartments (1 = <5, 2 = 5-20, 3 = 20-100, 4

991 = >100 cells), giving an average overall score of 5-10 fields of view per section.

992 PAS stained sections were scored at 100X magnification, on percentage of

993 mucous-positive epithelial cells (1 = <1%, 2 = 1-20%, 3 = 20-50%, 4 = 50-100%),

994 of 5-10 fields of view per section.

995 ***Measurement of airway hyperresponsiveness***

996 A Flexivent system (Scireq, Montreal, Canada) was used to measure dynamic

997 resistance and compliance. Mice were anaesthetised with intraperitoneal

998 ketamine 200 mg/kg and pentobarbitone (50 mg/kg), tracheotomised and

999 mechanically ventillated. Lung resistance and compliance were measured in

1000 response to nebulised methacholine (Sigma).

1001 *Immunoprecipitation:*

1002 Protein G dynabeads (Thermo Fisher) were coated with 5 μg anti-c-Myc (clone

1003 Myc.A7, Thermo Fisher), MOPC (IgG1 isotype control antibody) or ST2-Fc fusion

1004 protein (Biolegend), and washed on a DynaMag-2 magnet with PBS containing

1005 0.02% Tween 20. These were then used to immunoprecipitate HpARI-IL-33

1006 complexes, following manufacturer's instructions.

1007 Where human or mouse lung homogenates were used, these were prepared by

1008 homogenizing (Tissuelyser II, QIAGEN) one lung lobe (mouse) in 1 ml PBS, or

1009 400 mg human lung tissue in 1 ml PBS. Lung homogenates (100 ul) or 100 ng

1010 human or murine recombinant IL-33 (Biolegend) were then mixed with 1 μg

1011 HpARI in PBS containing 100 ug/ml OVA protein, and incubated for 30 min at

1012 37°C. Complexes were then added to coated dynabeads, incubated for 10 min at

1013 room temperature, and unbound material collected. Bound material on beads

1014 was washed 3 times in PBS+0.02% PBS on a DynaMag-2 magnet, before

1015 transferring to a fresh tube and eluting bound complexes using 50 mM glycine

1016 pH 2.8 (non-denaturing), before neutralising in 1M Tris buffer, pH 8. Eluted

1017 proteins and unbound supernatants were ran on 4-12% SDS-PAGE gels (Thermo

1018 Fisher) under non-reducing conditions, and transferred to nitrocellulose

1019 membranes for western blotting.

1020 *Surface Plasmon Resonance (SPR)*

1021 SPR measurements were performed using a BIAcore T200 instrument (GE

1022 Healthcare). Ni^{2+}-nitrilotriacetic acid (NTA) sensor chips were purchased from

1023 GE Healthcare. HpARI was immobilised on an NTA sensor surface to 400 RU,

1024 which gave essential zero baseline drift over the time course of the experiments

1025 performed: the apparent k- for the His-tagged HpARI Ni^{2+}-NTA surfaces was

1026   significantly slower than the complex being studied $\sim 5 \times 10^{-5}$ s^{-1} for HpARI-Ni-

1027   NTA *vs* $\sim 14\text{-}400 \times 10^{-5}$ s^{-1} for HpARI-IL-33, therefore short cycle (400-600 s total

1028   run times) single kinetic analysis could be reliably performed. Following Ni^{2+}

1029   priming (30 sec injection of 500 μM NiCl$_2$ at 5 µl·min^{-1}) 50 nM HpARI, in 10 mM

1030   NaH$_2$PO$_4$, pH 7.5; 150 mM NaCl; 50 μM EDTA; 0.05% surfactant P20, was

1031   captured *via* the 6-His tag by injection for 15 seconds, at 30 µl·min^{-1}. Surface

1032   regeneration between cycles and/or experiments was performed by dissociating

1033   any immobilised His-tagged protein or complex by a 90 s injection of 350 mM

1034   EDTA, in 10 mM NaH$_2$PO$_4$, pH 7.5; 150 mM NaCl; 0.05% surfactant P20 followed

1035   by a 30 s injection of 50 mM NaOH at the same flow rate.

1036   SPR kinetic titration binding experiments were performed at 25°C. Three-fold

1037   dilution series of mIL-33 (6.2 nM to 167 nM) or hIL-33 (0.062 µM to 1.67 µM),

1038   were injected over the sensor surface, in 10 mM NaH$_2$PO$_4$, pH 7.5; 150 mM NaCl;

1039   50 μM EDTA; 0.05% surfactant P20, at 30 µl.min^{-1} for 30 s followed by a 60 s

1040   dissociation phase. The same concentration series of mIL-33/hIL-33 were ran

1041   over Ni^{2+}-charged NTA surfaces, and showed no evidence of non-specific

1042   interaction of mIL-33/hIL-33 interacting with these surfaces. All experiments

1043   were performed on Ni^{2+}-charged surfaces following non-specific binding

1044   assessment and were double referenced using similar blank surface responses

1045   for run-noise corrections. The on- (k_+) and off-rate (k_-) constants and the

1046   equilibrium dissociation constant (K_d) were calculated by global fitting all three

1047   surfaces simultaneously to a 1:1 interaction model, with mass transport

1048   considerations, to the double reference corrected sensorgrams, using analysis

1049   software (v.2.01, GE Healthcare) provided with the BIAcore T200 instrument.

1050   Both interactions were extremely well fit by a simple 1:1 interaction model (Chi^2

1051   values of 0.457 and 0.395, mIL-33 and hIL-33 respectively), with RUmax values

1052   close to the theoretical maximum expected for a 1:1 stoichiometric interaction

1053   with high specific activity ($\sim$ 180 RU; 173 RU and 169.3 RU, mIL-33 and hIL-33

1054   respectively) and showed no evidence of mass transport issues.

1055

1056   ***Human lung explant culture***

1057   Approximately 5 g of lung tissue was washed 3 times in PBS and $\sim$0.5 mm^2 tissue

1058   explants prepared using sterilized scissors. Explants were incubated in 400 µl

1059   PBS+0.1% BSA +/- 10 µg/ml HpARI in wells of a 48-well tissue culture plate

1060   (Costar) for 1 h, at 37°C, 5% CO_2. Each condition was performed with 8 replicates

1061   for IL-33 measurement by ELISA, and pairs of supernatants were pooled (to

1062   make 4 replicates) for IL-33 western blot. After culture, tissue pieces were

1063   weighed, and IL-33 levels calculated relative to tissue weight.

1064   ***Gel shift assay***

1065   Linearized Not-HF-cut pSecTAG2A plasmid (10 ng) was mixed with HpARI,

1066   CCP1/2 and CCP2/3 proteins, in 10 mM TrisCl, 1 mM EDTA, and incubated for 30

1067   min at 37°C. Complexes were ran on a 0.7% agarose gel and imaged with Gelred

1068   (Biotium).

1069

1070   ***QUANTIFICATION AND STATISTICAL ANALYSIS***

1071   All data was analyzed using Prism (Graphpad Software Inc.). Where two groups

1072   were compared, Student's t-test was used, where there were 3 or more groups,

1073   one-way ANOVA with a Bonferroni's post test was used, and for comparing

1074   groups at multiple timepoints two-way ANOVA with a Sidak's post test was used.

1075   **** = p<0.0001, *** = p<0.001, ** = p<0.01, * = p<0.05, N.S. = Not Significant

1076   (p>0.05).

1077

1078

1079

KEY RESOURCES TABLE

REAGENT or RESOURCE	SOURCE	IDENTIFIER
Antibodies		
Anti-mouse CD3 (clone 145-2C11)	Biolegend	100306
Anti-mouse CD4 (clone RM4.5)	Biolegend	100566
Anti-mouse CD5 (clone 53-7.3)	Biolegend	100606
Anti-mouse CD11b (clone M1/70)	Biolegend	101224
Anti-mouse CD11c (clone N418)	Biolegend	117312
Anti-mouse CD19 (clone 6D5)	Biolegend	11506
Anti-mouse CD25 (clone PC61)	Biolegend	102038
Anti-mouse CD45 (clone 30-F11)	Biolegend	103128
Anti-mouse CD49b (clone DX5)	eBioscience	11-5971-85
Anti-mouse CD127 (clone A7R34)	Biolegend	135013
Anti-mouse ICOS (clone 15F9	eBioscience	46-9940-82
Anti-mouse GR1 (clone RB6-8C5)	Biolegend	108406
Anti-mouse IL-5 (clone TRFK5	Biolegend	504304
Anti-mouse IL-13 (clone eBio13A)	eBioscience	25-7133-82
Anti-mouse Ly6G (clone 1A8)	Biolegend	127616
Anti-mouse SiglecF (clone ES22-10D8)	Miltenyi	130-102-274
Anti-mouse ST2 (clone RMST2-2)	eBioscience	17-9335-82
Anti-mouse TER119 (clone TER-119)	Biolegend	116220
Anti-HMGB-1 rabbit polyclonal	Abcam	Ab18256
Anti-c-myc (clone Myc.A7)	Thermo Fisher Scientific	MA1-21316
Anti-human IL-33 goat polyclonal	R&D Systems	AF3625
Anti-mouse IL-33 goat polyclonal	R&D Systems	AF3626
Anti-mouse IL-1α	R&D Systems	AF-400-NA
IgG1 isotype control antibody (clone MOPC-21)	Produced in-house	N/A
Bacterial and Virus Strains		
Heligmosomoides polygyrus	(Johnston et al, 2015)	N/A
Nippostrongylus brasiliensis	(Lawrence et al, 1996)	N/A
Biological Samples		
Human lung tissue	Lothian NRS Bioresource	15/ES/0094
Chemicals, Peptides, and Recombinant Proteins		
Recombinant mouse IL-1α	Biolegend	575002
Recombinant mouse IL-33	Biolegend	580506
Recombinant human IL-33	Biolegend	581806
ST2-Fc	Biolegend	557904
Dynabeads Protein G	Thermo Fisher Scientific	10004D
Proteinase K	Sigma	557904
DNAse (protease-free)	Sigma	4536282001
Liberase TL	Sigma	05401020001
Methylcholine chloride	Sigma	A2251
Hoescht 33342	Thermo Fisher Scientific	H3570
Critical Commercial Assays		
Mouse IL-33 Duoset ELISA	R&D systems	DY3626

Human IL-33 Duoset ELISA	R&D systems	DY3625B
Annexin V Apoptosis Detection Kit	eBioscience	88-8005-72
Limulus Amoebocyte Lysate assay	Lonza	QCL-1000
Deposited Data		
Experimental Models: Cell Lines		
HEK293T	ATCC	CRL-3216
CMT-64	ECACC	10032301
Experimental Models: Organisms/Strains		
Mouse: IL-13-eGFP (C57BL/6J)	(Neill et al., 2010)	N/A
Mouse: hIL-33$^{+/+}$ / mIL-33$^{-/-}$ (humanized IL-33) (BALB/c)	(Cohen et al., 2015)	N/A
Oligonucleotides		
Recombinant DNA		
pSecTAG2A plasmid	Thermo Fisher Scientific	V90020
Software and Algorithms		
ClustalX	(Thompson et al., 1997)	www.clustal.org
Mascot v2.4	Matrix Science	www.matrixscience.com
SMART	(Letunic et al., 2015)	smart.embl-heidelberg.de/
HHpred	(Soding, 2005)	toolkit.tuebingen.mpg.de/#/tools/hhpred
Modeller v9.12	(Sali and Blundell, 1993)	salilab.org/modeller/
APBS	(Baker et al, 2001)	www.poissonboltzmann.org/
ESPript v3	(Robert and Gouet, 2014)	espript.ibcp.fr/
PyMOL	Schrödinger, LLC	www.pymol.org
PROSITE	(de Castro et al., 2006)	prosite.expasy.org/
Protein Data Bank	(Berman et al., 2000)	www.rcsb.org/pdb
Wormbase ParaSite	(Howe et al., 2016)	parasite.wormbase.org/
FlowJo v9.1	Flowjo, LLC	www.flowjo.com/
Prism v7	Graphpad Software	www.graphpad.com/scientific-software/prism/
BIAcore T200 software v2.01	GE Healthcare	N/A
Other		
Superdex 200 10/300 GL	GE Healthcare	17517501
MonoQ 5/50 GL	GE Healthcare	17-5166-01
Series S Sensor Chip NTA	GE Healthcare	BR-1005-32

Figure 1
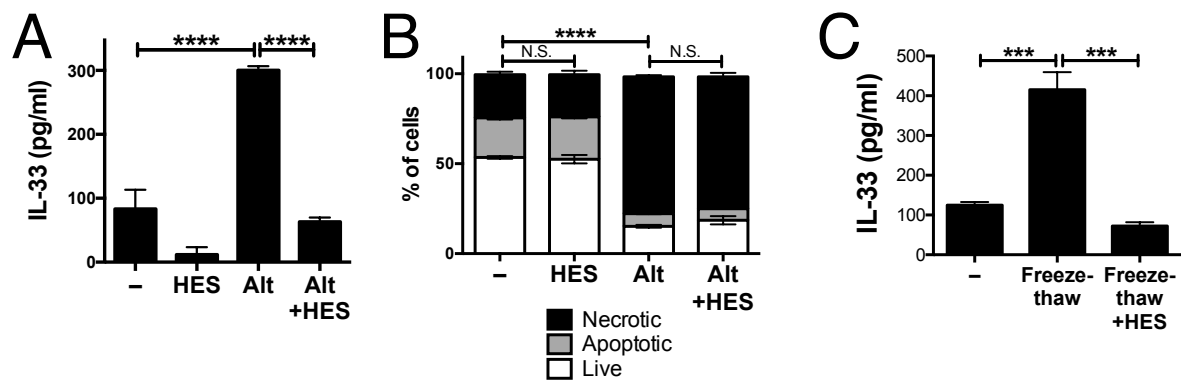
Figure 2
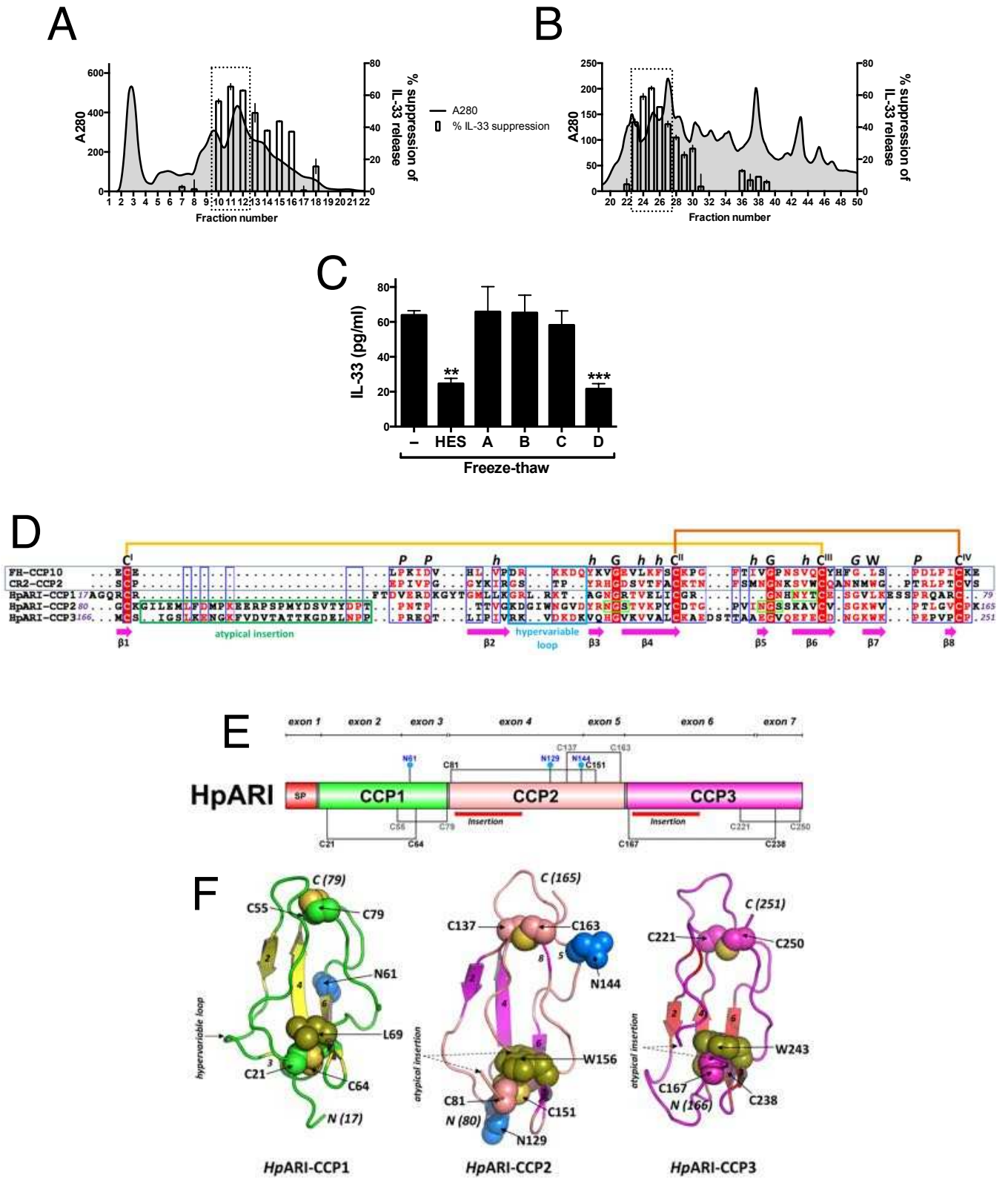
Figure 3
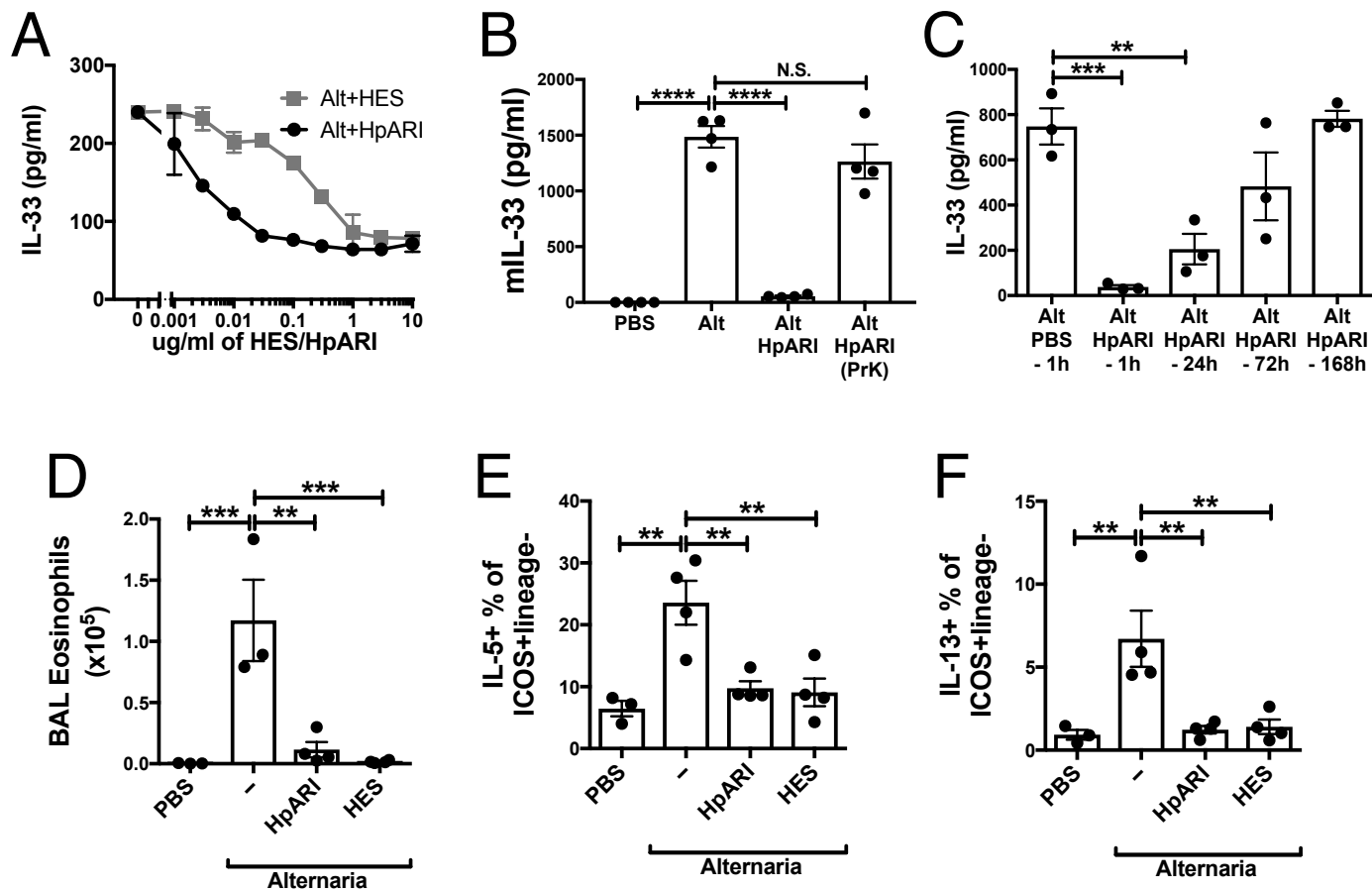
Figure 4
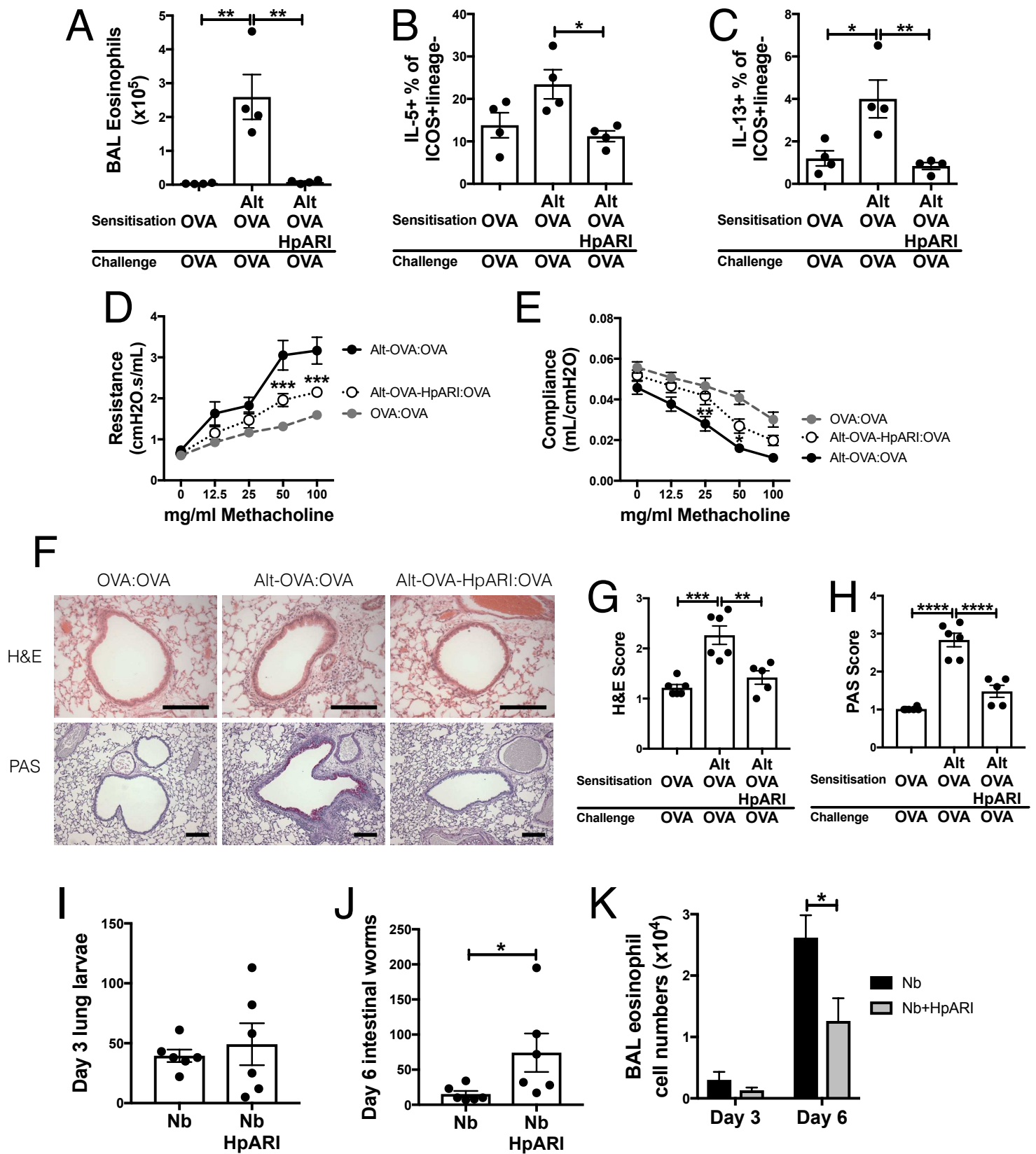
Figure 5
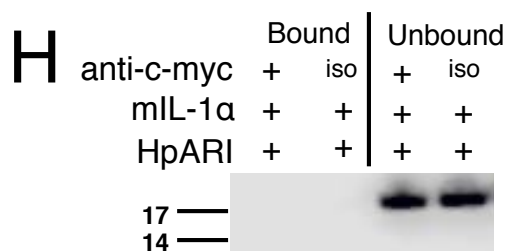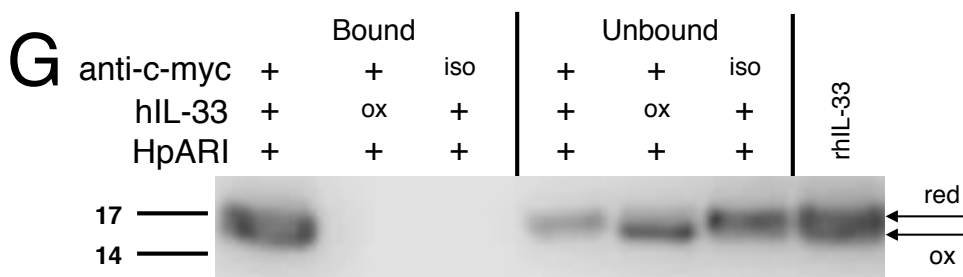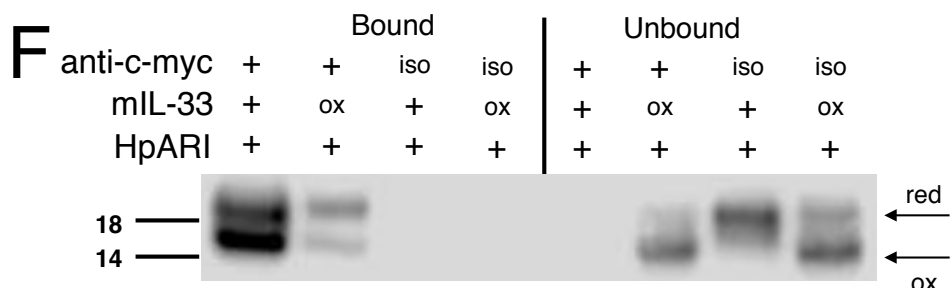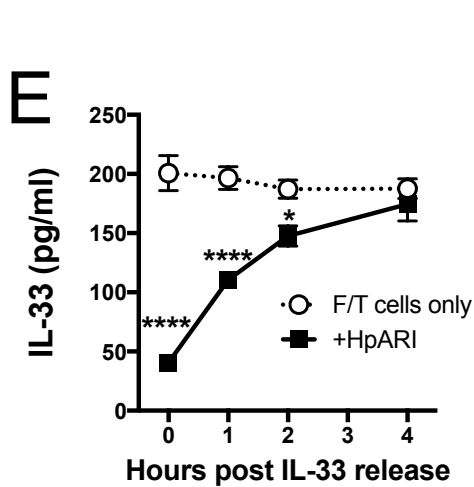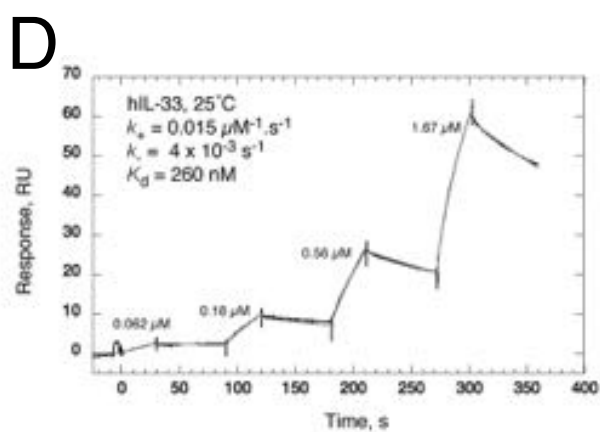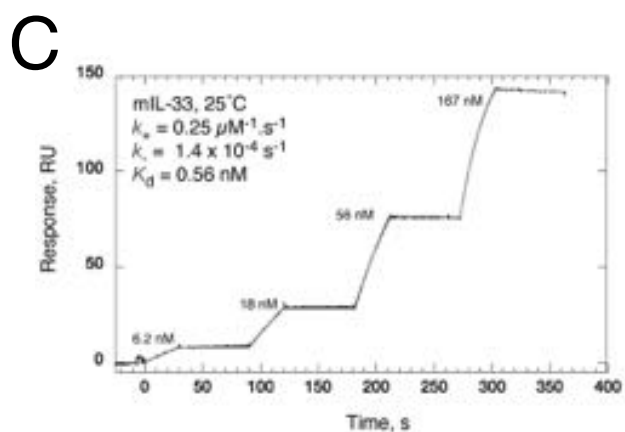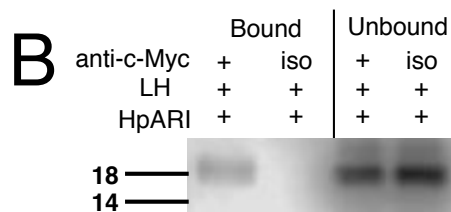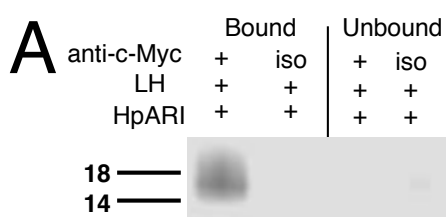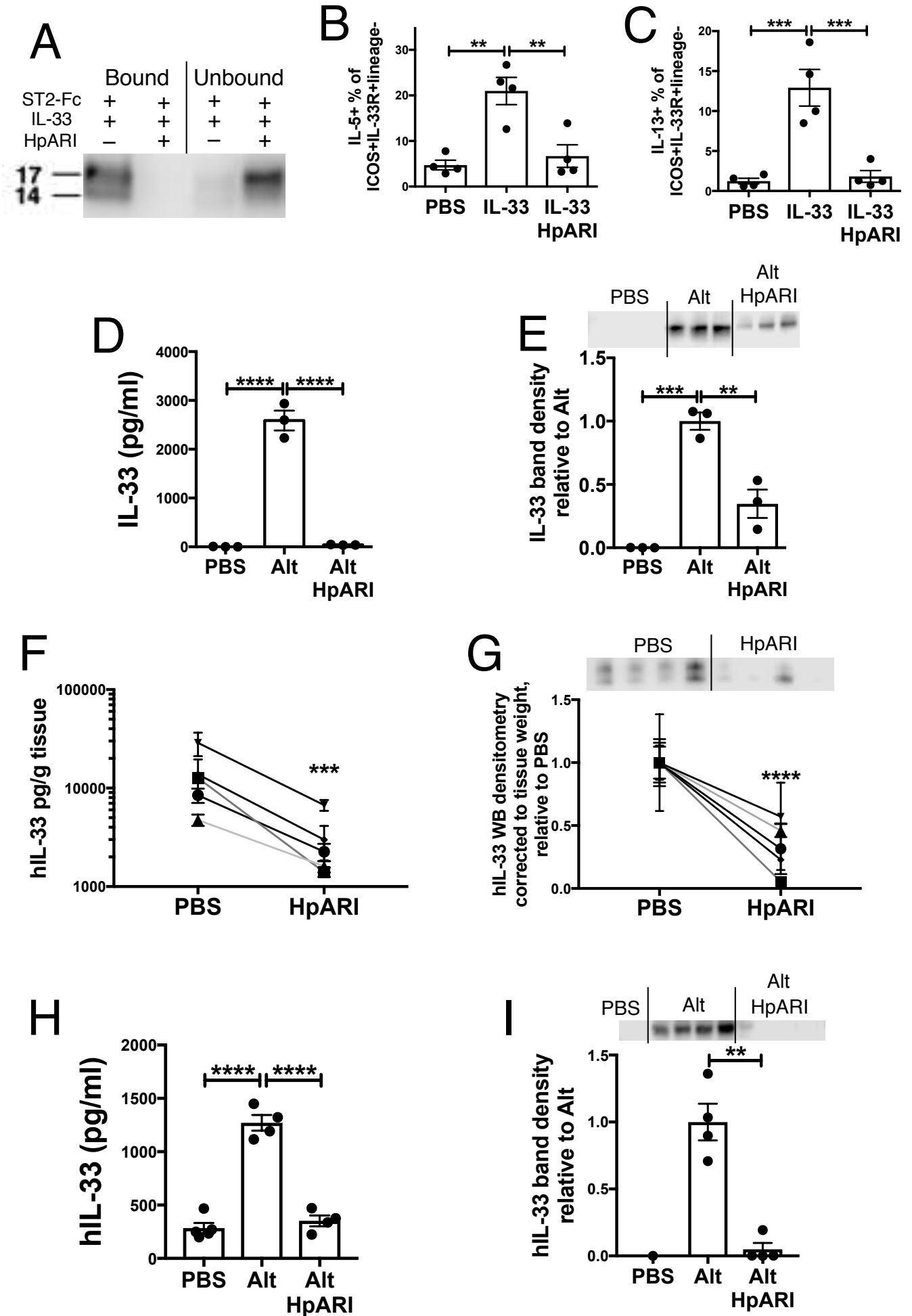
Figure 6

Figure 7
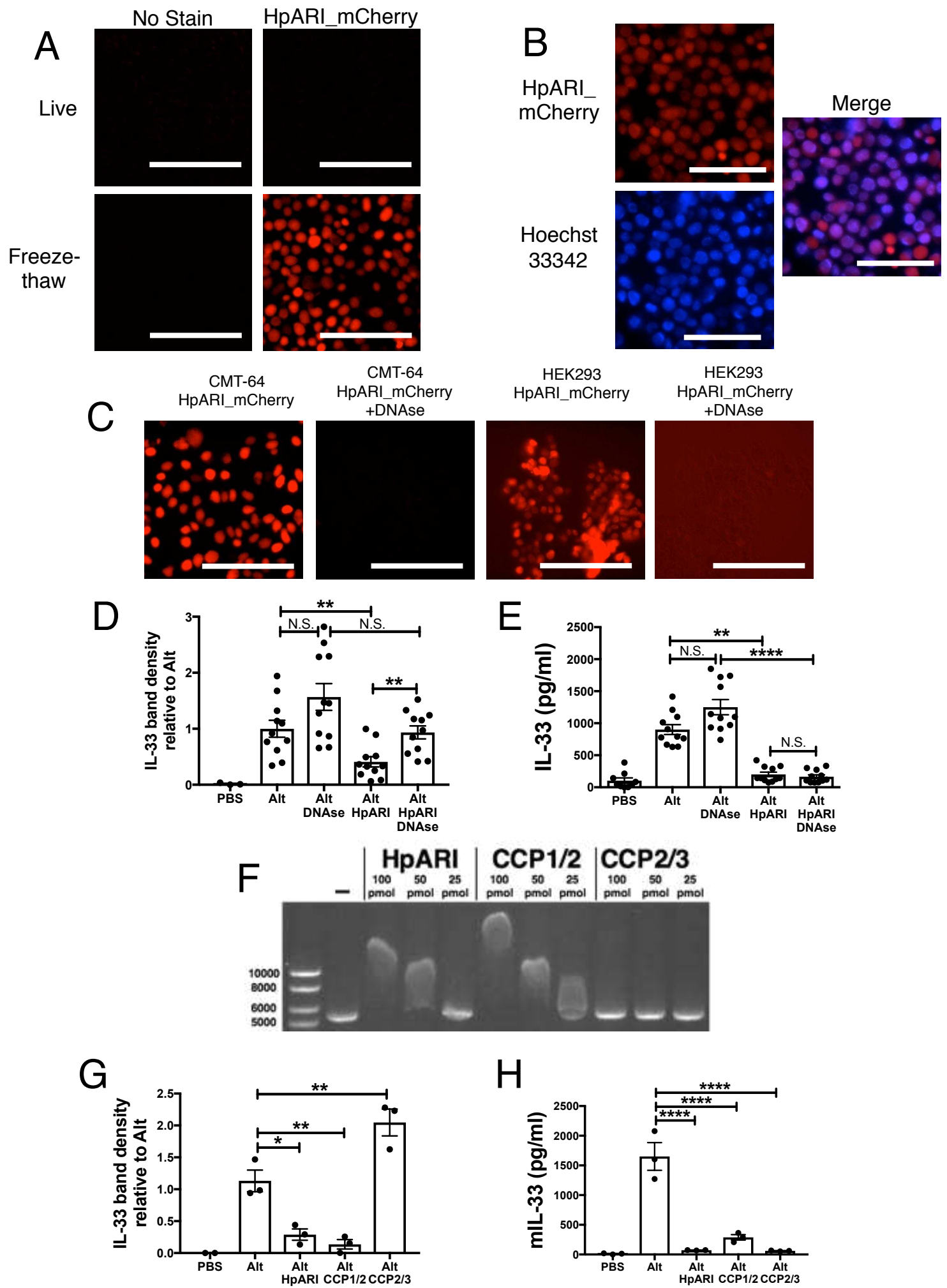
	Blast hit	Size fraction 11			Charge fraction 25		
		emPAI	Mascot protein score	Rank (of 194) [a]	emPAI	Mascot protein score	Rank (of 262) [a]
Hp_I10793_IG03481_L623	No BLASTX similarities 13330478:13331100 forward	1.35	99	57	0.53	104	77
Hp_I15874_IG07818_L1106	BLASTX similarity to 66.67% ID to CBN-NUC-1 protein [Caenorhabditis brenneri] (376 aa, Accession: gi|341901954|gb|EGT57889.1|)	1.11	229	19	5.23	786	2
Hp_I46029_IG37973_L313	BLASTX similarity to 55.93% ID to unnamed protein product [Homo sapiens] (304 aa, Accession: gi|189069304|dbj|BAG36336.1|)	2.01	67	90	0.73	50	163
Hp_I08176_IG02172_L1157	BLASTX similarity to 72.38% ID to PHA domain [Heligmosomoides polygyrus bakeri] (252 aa, Accession: gi|345499002|emb|CCC54333.1|)	0.13	61	100	1.05	353	18
GSXTT4C07IB13H_length=463	BLASTX similarity to 86.32% ID to venom allergen/ancylostoma secreted protein-like 1 isoform 4 [Heligmosomoides polygyrus bakeri] (459 aa, Accession: gi|348659354|gb|AEP82914.1|)	0.53	59	105	2.58	246	1
Hp_I00796_IG00050_L1763	BLASTX similarity to 60.51% ID to metalloprotease 1 precursor [Ancylostoma ceylanicum] (547 aa, Accession: gi|23268453|gb|AAN11401.1|)	0.37	163	32	0.78	518	3
Hp_I03365_IG00388_L986	BLASTX similarity to 83.05% ID to putative ES protein F7 [Ostertagia ostertagi] (181 aa, Accession: gi|18104159|emb|CAD20464.1|)	0.2	73	80	3.37	408	14
Hp_I05355_IG00918_L1570	BLASTX similarity to 61.84% ID to astacin-like metalloprotease [Haemonchus contortus] (502 aa, Accession: gi|82653303|emb|CAJ43810.1|)	0.51	205	20	0.34	137	20
Hp_I07496_IG01832_L2183	BLASTX similarity to 49.47% ID to metalloprotease I [Ostertagia ostertagi] (573 aa, Accession: gi|25005280|emb|CAD28559.2|)	0.23	184	24	0.52	300	26
Hp_I09193_IG02681_L996	BLASTX similarity to 27.72% ID to Chain A, Caclcium-Bound Ac-Asp-7 (206 aa, Accession: gi|383875397|pdb|3S6U|A)	0.2	78	72	1.28	312	24
Hp_I09338_IG02753_L893	BLASTX similarity to 69.57% ID to Chain A, Glutathione Transferase-2, Apo Form, From The Nematode Heligmosomoides Polygyrus (206 aa, Accession: gi|51247756|pdb|1TW9|A)	0.36	81	60	0.23	90	59
Hp_I12757_IG04701_L2227	BLASTX similarity to 69.27% ID to hypothetical protein CAEBREN_19315 [Caenorhabditis brenneri] (713 aa, Accession: gi|341886485|gb|EGT42420.1|)	0.9	321	9	0.29	119	67
Hp_I12915_IG04859_L2071	BLASTX similarity to 74.56% ID to hypothetical protein CAEBREN_01953 [Caenorhabditis brenneri] (594 aa, Accession: gi|341889762|gb|EGT45697.1|)	0.25	146	39	0.43	190	39
Hp_I13075_IG05019_L1949	BLASTX similarity to 25.30% ID to GD14343 [Drosophila simulans] (699 aa, Accession: gi|195589672|ref|XP_002084573.1|)	0.71	317	10	1.15	478	8
Hp_I13426_IG05370_L1731	BLASTX similarity to 61.51% ID to hexokinase [Haemonchus contortus] (485 aa, Accession: gi|4583627|emb|CAB40412.1|)	1.51	564	4	0.81	409	13
Hp_I13832_IG05776_L1555	BLASTX similarity to 59.25% ID to metalloprotease III [Ostertagia ostertagi] (507 aa, Accession: gi|21425408|emb|CAD19995.2|)	0.6	152	38	0.9	340	20
Hp_I14648_IG06592_L1319	No BLASTX similarities 18271778:18273096 forward	1.67	280	15	0.75	180	41
Hp_I14766_IG06710_L1294	BLASTX similarity to 42.09% ID to Hyaluronidase-1, partial [Ascaris suum] (439 aa, Accession: gi|324516157|gb|ADY46439.1|)	0.15	57	109	0.42	96	86
Hp_I15012_IG06956_L1244	BLASTX similarity to 71.51% ID to hypothetical protein CRE_02222 [Caenorhabditis remanei] (368 aa, Accession: gi|308509410|ref|XP_003116888.1|)	0.56	167	21	0.25	138	57
Hp_I15720_IG07664_L1128	BLASTX similarity to 83.79% ID to hypothetical protein CRE_30062 [Caenorhabditis remanei] (425 aa, Accession: gi|308473183|ref|XP_003098817.1|)	0.5	180	26	0.28	88	99
Hp_I15761_IG07705_L1121	BLASTX similarity to 78.44% ID to hypothetical protein CAEBREN_23086 [Caenorhabditis brenneri] (322 aa, Accession: gi|341889746|gb|EGT45681.1|)	0.18	41	144	1.47	368	16
Hp_I16083_IG08027_L1071	BLASTX similarity to 28.20% ID to Complement factor H [Ascaris suum] (1358 aa, Accession: gi|324499597|gb|ADY39830.1|)	0.41	72	85	0.19	42	186
Hp_I28418_IG20362_L498	BLASTX similarity to 45.24% ID to hypothetical protein CRE_02231 [Caenorhabditis remanei] (147 aa, Accession: gi|308510374|ref|XP_003117370.1|)	0.43	42	141	0.43	67	122
Hpb-APY-2	No BLASTX analysis performed; (File Apyrase 124-3 (iso 07051) 081110) 1062 nt	5.9	654	2	0.3	58	137
Hpb-GST-2	No BLASTX analysis performed; partial (no N-terminus) AF128959	1.07	96	60	0.79	138	59

a) Rank of 194 proteins in size fraction 11 or 262 candidates in charge fraction 25 determined by Mascot score, with a minimum score of 20

Supplementary Table 1 (related to Figure 1):
Candidate genes with emPAI peaking in size fractions 10-12 and charge fraction 23-27. Data shown for peak IL-33 suppressive fraction (size = 11, charge = 25).
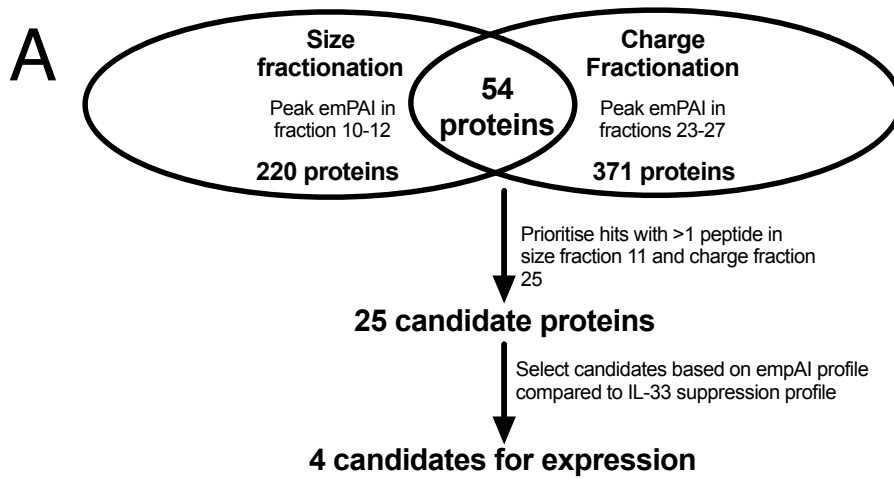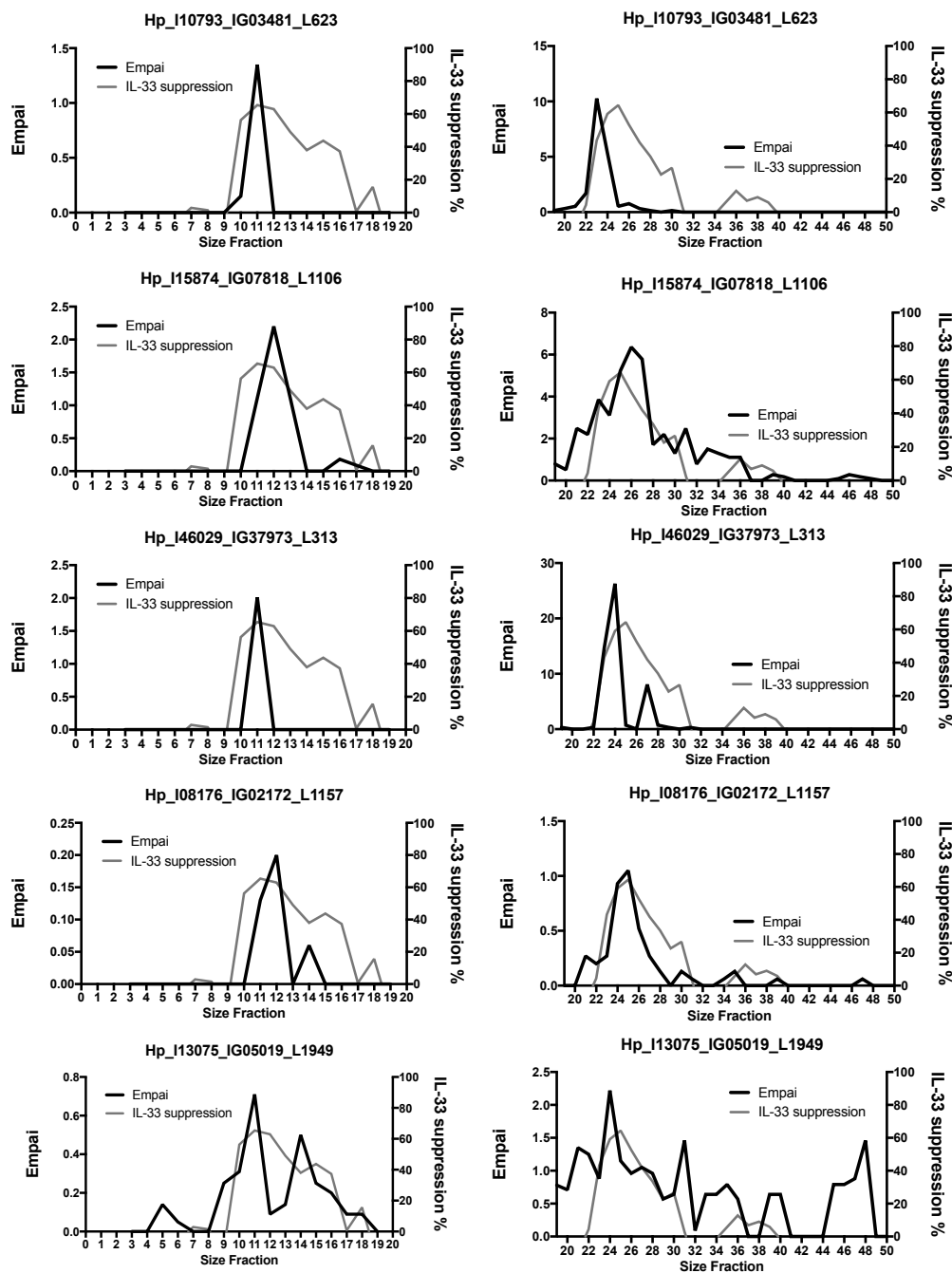
Supplementary Figure 1 (Related to Figure 1):

A. Candidate protein selection strategy

B. Candidate protein Empai profile and IL-33 suppression profile in HES size (left panels) and charge (right panels) fractions. The 4 candidate proteins tested in Fig 2A are shown followed by a candidate not selected for further testing (Hp_I13075_IG05019_L1949), for comparison.

A

```
0    atgtatcgcctttttctcgctttaggcttcctcaccttcatcaacgctgcaggtcagcgc   60
0     M  Y  R  L  F  L  A  L  G  F  L  T  F  I  N  A  A  G  Q  R    20

61   tgcagattcaccgatgtagaaagagacaaaggctacactggaatgctccttaaaggaagg  120
21    C  R  F  T  D  V  E  R  D  K  G  Y  T  G  M  L  L  K  G  R    40

121  ttaagaaagacagctggaaacgggaggacggtagaattgatatgtggaagaggaaatcac  180
41    L  R  K  T  A  G  N  G  R  T  V  E  L  I  C  G  R  G  N  H    60

181  aactacacctgcgagtccggcgttttgaaggaaagttctccacggcaagcccgatgtggt  240
61    N  Y  T  C  E  S  G  V  L  K  E  S  S  P  R  Q  A  R  C  G    80

241  tgcaagggaattctcgaaatgctcttcgatatgcctaaggaagaacggccctcgcccatg  300
81    C  K  G  I  L  E  M  L  F  D  M  P  K  E  E  R  P  S  P  M    100

301  tacgactcagtcacctatgaccccacgcccaacacccaacaactgtaggaaaggacggg   360
101   Y  D  S  V  T  Y  D  P  T  P  N  T  P  T  T  V  G  K  D  G    120

361  atatggaacggagtagattaccgcaatggctctacagtgaagccttattgcgatactggt  420
121   I  W  N  G  V  D  Y  R  N  G  S  T  V  K  P  Y  C  D  T  G    140

421  ccagtcatcaacggatcatccaaagctgtatgtgtgagtggcaaatgggttcctacgctt  480
141   P  V  I  N  G  S  S  K  A  V  C  V  S  G  K  W  V  P  T  L    160

481  ggcgtctgcccaaaaatgtgttcgatcggcagcttgaaggaaaatgggaaattcgtagac  540
161   G  V  C  P  K  M  C  S  I  G  S  L  K  E  N  G  K  F  V  D    180

541  gtcacagcaacaactaaaggagacgagctcaacccccccgccaagggaacagacattgatt  600
181   V  T  A  T  T  K  G  D  E  L  N  P  P  P  R  E  Q  T  L  I    200

601  cctatagtgcgtaaagttgacaaagacaaggtccaacacggcgtcaaagttgttgctctt  660
201   P  I  V  R  K  V  D  K  D  K  V  Q  H  G  V  K  V  V  A  L    220

661  tgtaaagccgaagattctacaactgccgctgaaggcgtccaggaattcgaatgtgacaac  720
221   C  K  A  E  D  S  T  T  A  A  E  G  V  Q  E  F  E  C  D  N    240

721  gggaagtggaagccagagcccgtgccctgcccctaa   756
241   G  K  W  K  P  E  P  V  P  C  P  -    251
```

B
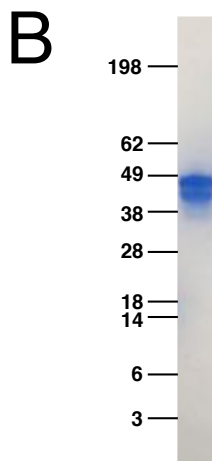
Supplementary Figure 2 (Related to Figure 2):

A. HpARI cDNA sequence showing intron/exon boundaries (green/yellow highlight) and amino acid domains (coloured boxes/text, red = signal peptide, green = CCP1, salmon = CCP2, pink = CCP3)

B. Coomassie-stained purifed HpARI (2 µg), purified by nickel affinity chromatography.
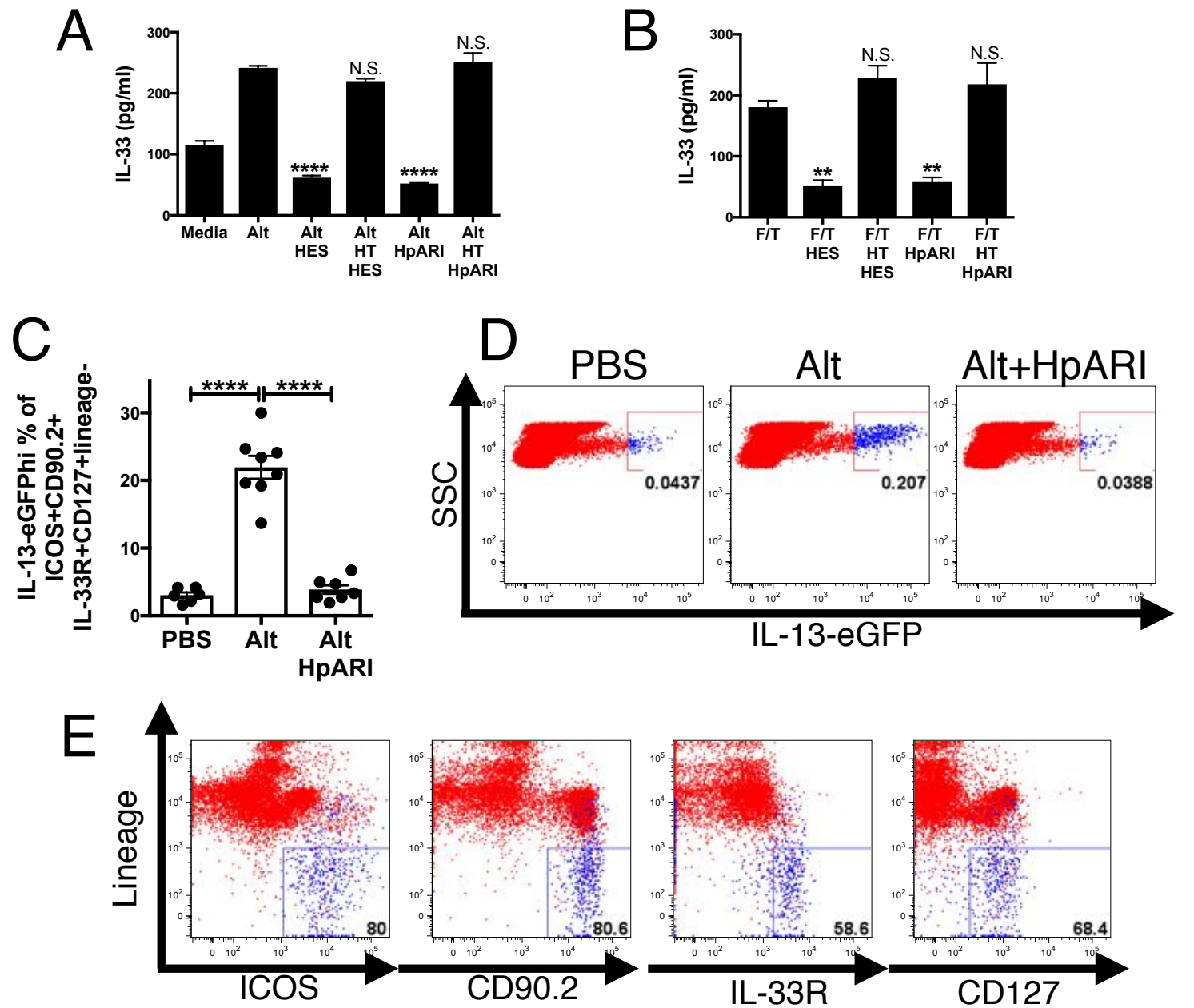
Supplementary Figure 3 (Related to Figure 3):

(A)   Naive mouse lung cells were cultured in the presence of Alternaria (200 µg/ml) and 10 µg/ml HES or HpARI for 1 h or heat-treated (95°C for 30 min) HES or HpARI (HT HES or HT HpARI). IL-33 in supernatants was measured by ELISA.

(B)   Naive murine lung cells were subjected to freeze/thaw treatment (F/T) in the presence of HES, HpARI, HT HES or HT HpARI. IL-33 in supernatants was measured by ELISA.

$****$ = p< 0.0001, $**$ = p<0.01, N.S. = Not significant (p>0.05), compared to Alternaria or freeze/thaw (F/T) control. Standard error of means of 3 replicates, representative of 2-3 repeat experiments.

(C)   IL-13-eGFP^{hi} proportion of ICOS+CD90.2+IL-33R+CD127+lineage– ILC2s in the lung, 24 h after intranasal administration of Alternaria allergen and HpARI to IL-13-eGFP reporter mice. Results pooled from 2 repeat experiments. $****$ = p< 0.0001

(D)   Representative FACS plots of IL-13-eGFP in live CD45+ lung lymphocytes from mouse shown in (C)

(E)   Representative FACS plots of IL-13-eGFP^{hi} cells (blue) and total CD45+ live lung lymphocytes (red) from an Alternaria-treated IL-13-eGFP reporter mouse.
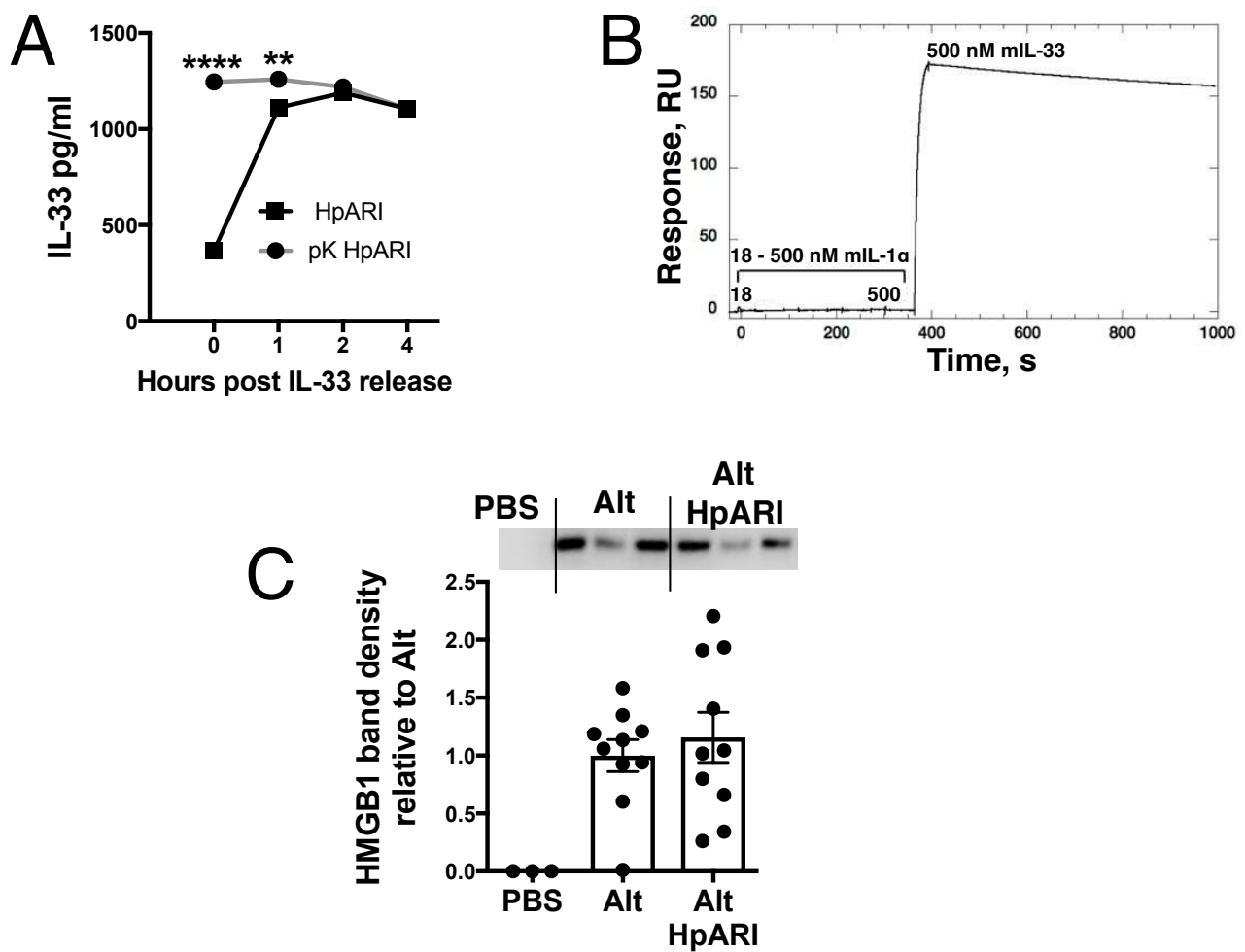
Supplementary Figure 4 (Related to Figure 5):
(A) CMT-64 cell supernatants were taken after freeze-thaw and treated with HpARI or proteinase K-digested and heat-treated HpARI over a timecourse after thaw, as in Figure 5C
(B) Surface plasmon resonance was carried out using mIL-1a or mIL-33 as a ligand for HpARI.
(C) HMGB1 western blots taken 15 min after Alternaria+/- HpARI administration. Pooled from 3 replicate experiments.
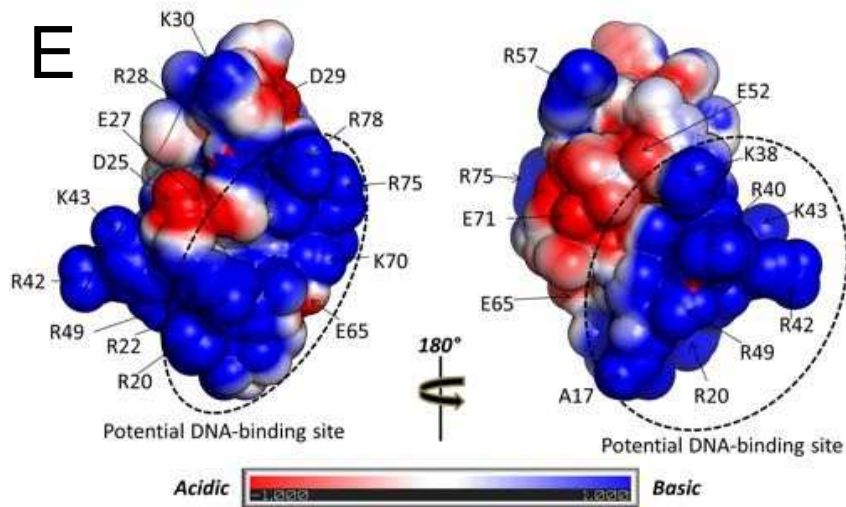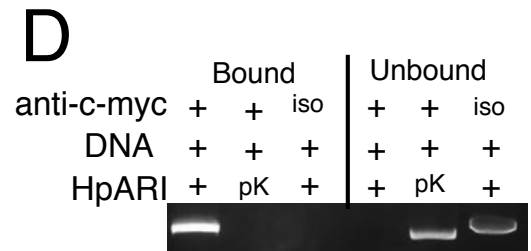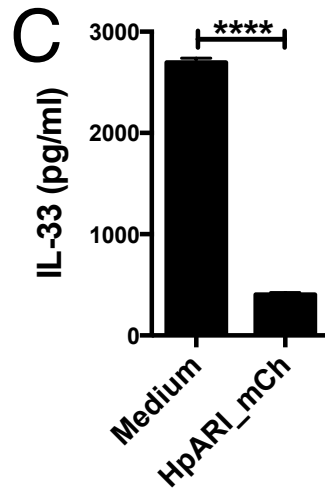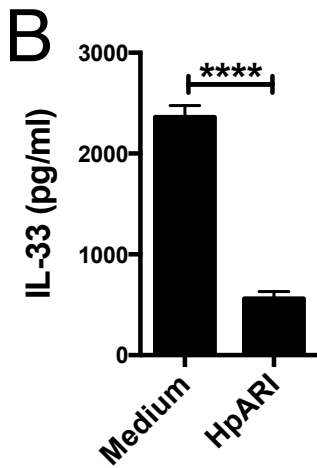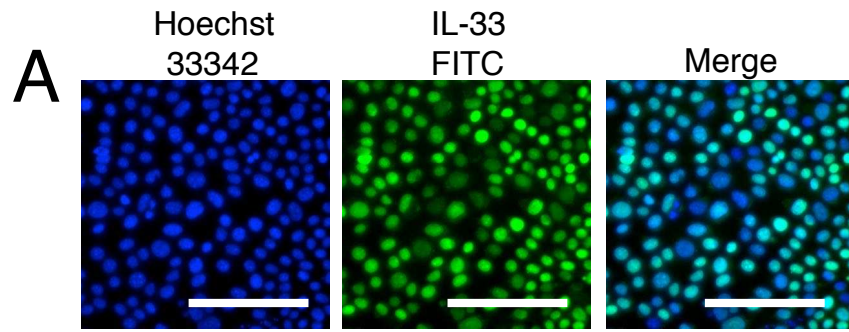
Supplementary Figure 5 (Related to Figure 7):
(A) CMT-64 cells were fixed and permeabilised, before staining with goat anti-mouse IL-33, followed by rabbit anti-goat IgG FITC secondary and counterstained with Hoechst 33342 nuclear stain. Scale bars indicate 100 μm.
(B) CMT-64 cells were subjected to freeze/thaw necrosis in the presence of 5 μg/ml HpARI and IL-33 in the supernatant measured by ELISA.
(C) CMT-64 cells were subjected to freeze/thaw necrosis in the presence of 5 μg/ml HpARI_mCherry and IL-33 in the supernatant measured by ELISA. **** = p<0.0001
(D) Immunoprecipitation of plasmid DNA by myc-tagged HpARI, but not by proteinase K and heat treated HpARI (pK) nor with isotype control antibody.
(E) Two views rotated by 180° along the y-axis depicting the electrostatic surface map of the 3-D model of HpARI CCP1 (calculated using APBS) revealing key residues contributing to the highly basic surface (coloured blue) that may confer DNA-binding properties; acidic surface residues are shown in red. A scaled range of -1kT to +1 kT was used, where k=Boltzman's constant and T= Temperature in Kelvins.